Quasi-LPV modeling, identification and control of a twin rotor MIMO system

Article *in* Control Engineering Practice · June 2013

DOI: 10.1016/j.conengprac.2013.02.004

CITATIONS
84

READS
1,037

3 authors:

Damiano Rotondo
University of Stavanger (UiS)
124 PUBLICATIONS **1,525** CITATIONS
SEE PROFILE

Fatiha Nejjari
Universitat Politècnica de Catalunya
167 PUBLICATIONS **2,444** CITATIONS
SEE PROFILE

Vicenç Puig
Universitat Politècnica de Catalunya
720 PUBLICATIONS **8,958** CITATIONS
SEE PROFILE

Quasi-LPV Modeling, Identification and Control of a Twin Rotor MIMO System

Damiano Rotondo[a,*], Fatiha Nejjari[a], Vicenç Puig[a]

[a]*Department of Automatic Control (ESAII), Technical University of Catalonia (UPC), Rambla de Sant Nebridi 10, 08222 - Terrassa (Spain). Tel: +34 93 739 89 73*

Abstract

This paper describes the quasi-linear parameter varying (quasi-LPV) modeling, identification and control of a Twin Rotor MIMO System (TRMS). The non-linear model of the TRMS is transformed into a quasi-LPV system and approximated in a polytopic way. The unknown model parameters have been calibrated by means of the non-linear least squares identification approach and validated against real data. Finally, an LPV observer and state-feedback controller have been designed using an LPV pole placement method based on LMI regions. The effectiveness and performance of the proposed control approach have been proved both in simulation and on the real set-up.

Keywords: LPV, TRMS, Gain-Scheduling, Helicopter, LMIs, Polytopic Model

1. Introduction

This paper describes the quasi-linear parameter varying (quasi-LPV) modeling, identification and control of the Twin-Rotor Multiple-Input Multiple-Output system (TRMS), developed by Feedback Instruments Limited for control experiments. This system resembles a simplified behavior of a conventional helicopter with less degrees of freedom (DOF). The system is perceived as a challenging engineering problem owing to its high non-linearity, cross-coupling between its two axes, and inaccessibility of some of its states for measurements.

An attractive solution to represent nonlinear systems are LPV models. The main advantage of LPV models is that they allow applying powerful linear de-

*Corresponding author

Email addresses: damiano.rotondo@yahoo.it (Damiano Rotondo), fatiha.nejjari@upc.edu (Fatiha Nejjari), vicenc.puig@upc.edu (Vicenç Puig)

sign tools to complex nonlinear models (Reberga et al., 2005; Wan & Kothare, 2003; Rodrigues et al., 2007). LPV control synthesis fits into the gain scheduling framework, while adding stability and robustness guarantees. The strength of the LPV approach lies in the extension of well-known methods for linear optimal control, including the use of linear matrix inequalities (LMIs), to the design of gain scheduled LPV controllers. A condition to apply LPV control synthesis is to transform the nonlinear model of the system into an LPV model; hence, LPV modeling becomes a key issue in the design of LPV controllers (Papageorgiou, 1998; Shamma & Cloutier, 1993; Andrés & Balas, 2004). Luckily, many nonlinear systems of practical interest can be represented as quasi-LPV systems, where *quasi* is added because the scheduling parameters do not depend only on external signals, but also on system variables (Kwiatkowski et al., 2006). For further information about LPV systems, see Rugh & Shamma (2000), Toth et al. (2012) and the references therein.

The first development of LPV model identification methods focused on a global procedure, resulting in techniques that identify LPV models based on *one* set of measurements on the system with time-varying parameters. These techniques assume that one global experiment was enough to excite both the control inputs and the scheduling parameters (Nemani et al., 1995; Lee & Poolla, 1999; van Wingerden & Verhaegen, 2009). On the other hand, more recently, techniques that identify LPV models based on different sets of system measurements for different frozen values of the varying parameter have been investigated (Steinbuch et al., 2003; van Helvoort et al., 2004; Groot Wassink et al., 2005; Paijmans et al., 2008). These techniques start from a set of LTI identifications based on system measurements for a set of frozen values of the scheduling parameters. By interpolating between these local LTI models an LPV model is obtained.

In the last decade, the modeling and experimental identification of the TRMS have been investigated and addressed in many papers. Radial basis function networks were used in (Ahmad et al., 2000), where a non-linear modeling and identification approach was presented and applied to air vehicles of complex configuration. In (Ahmad et al., 2002), a black-box system identification technique was used to obtain a dynamic model for a 1DOF TRMS in hover. In (Darus et al., 2004), genetic algorithms based on one-step-ahead prediction were used to identify the parameters of the TRMS in hovering position. Shaheed (2004) obtained a model of the TRMS using a nonlinear autoregressive process with external input (NARX) paradigm with a feedforward neural network. In (Aldebrez et al., 2004), the utilization of neural networks and parametric linear approaches for modeling a TRMS in hovering position has been investigated. In (Alam & Tokhi, 2007),

particle swarm optimization is used to model the TRMS. First, 1DOF models are extracted for both vertical and horizontal channels, respectively. Then, a 2DOF parametric model is developed taking into consideration cross-couplings between the channels. In (Rahideh & Shaheed, 2007), the system is modeled in terms of vertical 1DOF, horizontal 1DOF and 2DOF dynamics using Newtonian as well as Lagrangian methods. Further improvements of such model can be found in (Gabriel, 2008), (Nejjari et al., 2011), and in (Rahideh et al., 2008), where, in addition, Levenberg-Marquardt and gradient descent neural network-based empirical models are obtained and compared to the Newtonian and Lagrangian analytical ones. In (Toha & Tokhi, 2009), the parametric modeling of the TRMS is obtained by means of real-coded genetic algorithm. In (Toha & Tokhi, 2010a), an adaptive neuro-fuzzy inference system tuned by a particle swarm optimization algorithm is developed in search for a non-parametric model of the TRMS. In (Toha & Tokhi, 2010b), a fourth-order linear auto-regressive moving average that describes the hovering motion of the TRMS is obtained by means of recursive least squares, genetic algorithms and particle swarm optimization.

Regarding the control of the TRMS, a non-linear predictive control has been presented in (Dutka et al., 2003). The non-linearity is handled by converting the state-dependent state-space representation into the linear time-varying representation. In (López-Martinez & Rubio, 2003) and (López-Martinez et al., 2004), the control of the twin rotor system using feedback linearization techniques (as full state linearization and input output linearization) has been suggested. In (López-Martinez et al., 2003), a H_∞ controller for helicopter dynamics is proposed. Later, a non-linear H_∞ approach for handling the coupling considered as a disturbance that should be rejected is introduced in (López-Martinez et al., 2005). The resulting controller exhibited attributes of a non-linear PID with time-varying constants according to the operating point. In (Ahmed et al., 2009), a sliding mode control by defining a sliding surface that allows to deal with cross-coupling inherent in the twin rotor dynamics is considered. In (Rahideh & Shaheed, 2009), the TRMS is controlled using robust model predictive control based on polytopes. In (Tao et al., 2010), a fuzzy-sliding and fuzzy-integral-sliding controller is designed to position the yaw and pitch angles of a TRMS.

The interest in LPV systems is motivated by their use in gain-scheduling control techniques. The possibility to embed nonlinear systems into the LPV framework, by hiding nonlinearities within the scheduling parameter, enables the application of linear-like control methods to nonlinear systems such that, at the same time, stability and desired performance of the closed-loop system are guaranteed.

The work presented in this paper is an improvement and an extension of (Ne-

jjari et al., 2011) and (Nejjari et al., 2012). In Nejjari et al. (2011), the model proposed by Rahideh & Shaheed (2007) was used as a starting point for obtaining a quasi-LPV representation of the TRMS to be used for the design of a state observer and a state-feedback controller. The proposed modeling and control approach was tested in simulation in order to prove its effectiveness and performance. In Nejjari et al. (2012), the parameters of the non-linear model were calibrated using data collected from the real lab set-up. The obtained model was used to derive a polytopic model that could be used for controlling the real set-up. In this paper, the modeling and identification techniques described in Nejjari et al. (2012) are used to obtain a polytopic model for a real TRMS. This model is used for controlling the real TRMS, thus showing that the approach proposed in Nejjari et al. (2011) can be successfully applied in practical control problems. In the current paper, the whole procedure is discussed in a more detailed and integrated way such that this paper could be used as a guide for solving the full LPV modeling/identification/control approach for the TRMS system, that can be extended to the control of other complex non-linear systems.

One of the contributions of this paper is the improvement of the nonlinear model of the TRMS proposed by Rahideh & Shaheed (2007) taking into account some coupling phenomena that were noticed during the identification process. Another contribution is the proposition of a way that permits transforming the TRMS nonlinear model into a discrete-time polytopic quasi-LPV model. The method presented in (Kwiatkowski et al., 2006) for an automated generation of affine LPV representations from nonlinear and parameter dependent systems is used. Including the TRMS model nonlinearities in an LPV framework leads to an improvement in the modeling accuracy and control performance of such a system. The resulting model is polytopic and quasi-LPV, and is used directly in the control strategy. Another contribution consists in using the so called *glocal* identification procedure (Mercere et al., 2011), to estimate a global quasi-LPV model of the TRMS from local experiments. Once the model is identified, the LPV control theory developed by Apkarian et al. (1995) is applied. This control methodology allows designing an LPV state feedback controller that automatically adapts to the operating point. Since not all the TRMS state variables are measured, an LPV observer is designed to estimate them. Finally, an important practical contribution of this work is the application of the proposed LPV modeling, identification and control approach to the real TRMS system. It should be stated that the Takagi-Sugeno (TS) modeling and control paradigm (Takagi & Sugeno, 1985) could alternatively be used for the control of the TRMS. According to Mäkilä & Viljamaa (2002), Bergsten et al. (2002) and Rong & Irwin (2003), polytopic LPV models and TS

models are very similar and probably the results obtained when applied to the TRMS would be very close.

The structure of the paper is the following: In Section 2, the Twin-Rotor MIMO System is described and its mathematical model is provided. In Section 3, a method for the automated generation of LPV models is applied so as to obtain the quasi-LPV model of the TRMS and the *bounding box* method is used to get a polytopic quasi-LPV representation that can be used for design purposes. Section 4 describes the identification approach used to estimate the unknown parameters of the TRMS model. Section 5 reviews the background on LPV control design using LMI pole placement and presents the design of the LPV state feedback controller and observer. Finally, the TRMS identification and control results are shown in Section 6 and the main conclusions are summarized in Section 7.

1.1. Nomenclature

Given a vector $\boldsymbol{v} \in \mathbb{R}^{n_v}$, its i^{th} element is denoted by v_i, with $i = 1, \ldots, n_v$. In case a lower and upper bound for v_i are known, they will be denoted as $\underline{v}_i$ and $\overline{v}_i$, respectively. Given a matrix $\mathbf{M}$, its elements are denoted by m_{ij}.

Most of the nomenclature used throughout the paper has been resumed in Tables 1-4, where the symbols are listed in alphabetical order (Latin alphabetical order first, followed by Greek alphabetical order). In case a symbol is not found in the tables, its meaning should be deducible from the text of the subsection where it appears.

2. Non-linear Model of the TRMS

The Twin-Rotor Multiple-Input Multiple-Output (MIMO) System is a laboratory aero-dynamical system, developed by Feedback Instruments for control experiments (see Fig. 1). The system is considered as a challenging engineering problem due to its high non-linearity, presence of cross-coupling between its axes, and inaccessibility of some of its states for measurements. In order to achieve control objectives satisfactorily, an accurate model of the system is needed (Rahideh & Shaheed, 2007).

The TRMS is similar in its behavior to a helicopter. At both ends of its beam there are two propellers driven by DC motors, each perpendicular to the other one. The beam can rotate freely in the horizontal and vertical planes, in such a way that its ends move on spherical surfaces. The joined beam can be moved by changing the motor supply voltages, thus controlling the rotational speed of the propellers. A counter-weight fixed to the beam is used for balancing the angular momentum

Table 1: Nomenclature

Symbol	Description
$\mathbf{A}$	state matrix in a state-space model
$\mathbf{A_d}$	discrete-time approximation of $\mathbf{A}$
$\mathbf{A}_i$	state matrix of the i^{th} vertex system
$\mathbf{B}$	input matrix in a state-space model
$\mathbf{B_d}$	discrete-time approximation of $\mathbf{B}$
$\mathbf{C}$	output matrix in a state-space model
$\mathbf{D}$	feedthrough matrix in a state-space model
$\mathcal{D}$	LMI region
$\mathbf{f}_{\mathcal{D}}(z)$	characteristic function of the LMI region $\mathcal{D}$
$\mathbf{K_d}$	gain of the discrete-time controller
$\mathbf{L_d}$	gain of the discrete-time observer
N	number of vertex system in a polytopic representation
$\boldsymbol{p}$	vector of system variables used to calculate $\boldsymbol{\psi}$ using $\mathbf{f}_{\psi}$
$\boldsymbol{p_d}$	discrete-time approximation of $\boldsymbol{p}(k)$
$\boldsymbol{r}$	reference
T_s	sample time
$\boldsymbol{u}$	input vector in a state-space model
$\boldsymbol{u_r}$	feedforward control action
$\mathbf{X}$	Lyapunov matrix
$\boldsymbol{x}$	state vector in a state-space model
$\hat{\boldsymbol{x}}$	estimated state
$\boldsymbol{x_r}$	state reference
$\boldsymbol{y}$	output vector in a state-space model
$\hat{\boldsymbol{y}}$	estimated output
$\mathbf{Z}_{\mathcal{D}}$	matrix obtained from the characteristic function $\mathbf{f}_{\mathcal{D}}(z)$
π_i	i^{th} coefficient of a polytopic decomposition
$\boldsymbol{\alpha}$	symmetric matrix in the characteristic function $\mathbf{f}_{\mathcal{D}}(z)$
$\boldsymbol{\beta}$	matrix in the characteristic function $\mathbf{f}_{\mathcal{D}}(z)$
$\boldsymbol{\psi}(.)$	varying parameter vector
$\boldsymbol{\psi_d}$	discrete-time approximation of $\boldsymbol{\psi}$

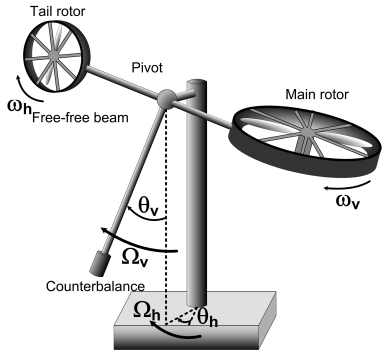

Figure 1: Components of the Twin Rotor MIMO System

in a stable equilibrium position. The rotor generating the vertical movement is called the main rotor. It enables the TRMS to pitch, which is a rotation in the vertical plane around the horizontal axes. The rotor generating the horizontal movement is called the tail rotor. It enables the TRMS to yaw, which is a rotation in the horizontal plane around the vertical axes.

The crude dynamic model of the system supplied by the manufacturer does not represent the system dynamics accurately, as all the effective forces are not taken into consideration. Accurate models are proposed by Rahideh & Shaheed (2007), Gabriel (2008) and Christensen (2006). Each of these models contemplates dynamical effects that have not been considered by the manufacturer, and leads to a set of non-linear differential equations. The strategy to describe the TRMS would be to split the system into simpler subsystems: the DC-Motors, the propellers and the beam. The first two have independent dynamics, that is, the main motor does not affect the behavior of the tail motor, and vice-versa. The same is true for the propellers. On the other hand, the dynamics of the beam is strongly non-linear with the presence of interaction phenomena among the horizontal and the vertical dynamics.

The model proposed by Rahideh & Shaheed (2007) has been modified by neglecting the electrical dynamics, by adding a function $f_6(\theta_v)$ that takes into account a coupling phenomenon noticed during the identification phase that was not explained by Rahideh's nonlinear model, and by replacing in the state vector the angular momenta in the horizontal and vertical plane S_h and S_v with the corresponding angular velocities Ω_h and Ω_v.

The TRMS non-linear model results in a set of 6 non-linear differential equations (see Nejjari et al., 2011):

$$\frac{d\omega_h}{dt} = \frac{k_a k_1}{J_{tr} R_a} u_h - \left(\frac{B_{tr}}{J_{tr}} + \frac{k_a^2}{J_{tr} R_a}\right)\omega_h - \frac{f_1(\omega_h)}{J_{tr}} \tag{1}$$

$$\begin{aligned}\frac{d\Omega_h}{dt} = {} & \frac{l_t f_2(\omega_h)\cos\theta_v - k_{oh}\Omega_h - f_3(\theta_h) + f_6(\theta_v)}{K_D\cos^2\theta_v + K_E\sin^2\theta_v + K_F} + \\ & \frac{k_m\omega_v\sin\theta_v\Omega_v\left(K_D\cos^2\theta_v - K_E\sin^2\theta_v - K_F - 2K_E\cos^2\theta_v\right)}{\left(K_D\cos^2\theta_v + K_E\sin^2\theta_v + K_F\right)^2} \\ & + \frac{k_m\cos\theta_v\left(\frac{k_a k_2}{R_a}u_v - \left(B_{mr} + \frac{k_a^2}{R_a}\right)\omega_v - f_4(\omega_v)\right)}{J_{mr}\left(K_D\cos^2\theta_v + K_E\sin^2\theta_v + K_F\right)}\end{aligned} \tag{2}$$

$$\frac{d\theta_h}{dt} = \Omega_h \tag{3}$$

$$\frac{d\omega_v}{dt} = \frac{k_a k_2}{J_{mr} R_a} u_v - \left(\frac{B_{mr}}{J_{mr}} + \frac{k_a^2}{J_{mr} R_a}\right)\omega_v - \frac{f_4(\omega_v)}{J_{mr}} \tag{4}$$

$$\begin{aligned}\frac{d\Omega_v}{dt} = {} & \frac{l_m f_5(\omega_v) + k_g\Omega_h f_5(\omega_v)\cos\theta_v - k_{ov}\Omega_v}{J_v} \\ & + \frac{g\left((K_A - K_B)\cos\theta_v - K_C\sin\theta_v\right) - {\Omega_h}^2 K_H\sin\theta_v\cos\theta_v}{J_v} \\ & + \frac{k_t\left(\frac{k_a k_1}{R_a}u_h - \left(B_{tr} + \frac{k_a^2}{R_a}\right)\omega_h - f_1(\omega_h)\right)}{J_v J_{tr}}\end{aligned} \tag{5}$$

$$\frac{d\theta_v}{dt} = \Omega_v \tag{6}$$

The system input vector is $\boldsymbol{u} = [u_h,\ u_v]^T$ while the system state vector is $\boldsymbol{x} = [\omega_h,\ \Omega_h,\ \theta_h,\ \omega_v,\ \omega_v,\ \theta_v]^T$. J_v is calculated as the sum of the following components:

$$J_{v1} = m_{mr} l_m^2 \tag{7}$$

$$J_{v2} = m_m l_m^2 \Big/ 3 \tag{8}$$

$$J_{v3} = m_{cb} l_{cb}^2 \tag{9}$$

$$J_{v4} = m_b l_b^2 \Big/ 3 \tag{10}$$

Table 2: TRMS parameters (part 1)

Symbol	Description
B_{mr}	viscous friction coefficient of the main propeller
B_{tr}	viscous friction coefficient of the tail propeller
$f_1(\omega_h)$	drag friction of the tail propeller, defined in (15)
$f_2(\omega_h)$	aerodynamic force due to the tail rotor, defined in (16)
$f_3(\theta_h)$	torque of the flat cable force, defined in (17)
$f_4(\omega_v)$	drag friction of the main propeller, defined in (18)
$f_5(\omega_v)$	aerodynamic force due to the main rotor, defined in (19)
$f_6(\theta_v)$	nonlinear coupling between θ_v and θ_h, defined in (20)
g	gravitational acceleration at sea level
J_{mr}	moment of inertia of the main propeller
J_{tr}	moment of inertia of the tail propeller
J_v	vertical moment of inertia
J_{v1}	main rotor component of J_v, defined in (7)
J_{v2}	beam of the main rotor component of J_v, defined in (8)
J_{v3}	counterweight component of J_v, defined in (9)
J_{v4}	beam of the counterweight component of J_v, defined in (10)
J_{v5}	tail rotor component of J_v, defined in (11)
J_{v6}	beam of the tail rotor component of J_v, defined in (12)
J_{v7}	shield of the main rotor component of J_v, defined in (13)
J_{v8}	shield of the tail rotor component of J_v, defined in (14)
K_A	physical constant defined in (21)
K_B	physical constant defined in (22)
K_C	physical constant defined in (23)
K_D	physical constant defined in (24)
K_E	physical constant defined in (25)
K_F	physical constant defined in (26)

Table 3: TRMS parameters (part 2)

Symbol	Description
K_H	physical constant defined in (27)
k_1	input constance of the tail motor
k_2	input constance of the main motor
k_a	torque constant of the DC motors
k_{chn}	cable force coefficient for negative θ_h
k_{chp}	cable force coefficient for positive θ_h
k_{cvn}	coupling coefficient for $\theta_v < \theta_v^0$
k_{cvp}	coupling coefficient for $\theta_v \geq \theta_v^0$
k_{fhn}	aerodynamic force coefficient of the tail rotor for negative ω_h
k_{fhp}	aerodynamic force coefficient of the tail rotor for positive ω_h
k_{fvn}	aerodynamic force coefficient of the main rotor for negative ω_v
k_{fvp}	aerodynamic force coefficient of the main rotor for positive ω_v
k_g	gyroscopic constant
k_m	positive constant
k_{oh}	horizontal friction coefficient of the beam subsystem
k_{ov}	vertical friction coefficient of the beam subsystem
k_{thn}	drag friction coefficient of the tail propeller for negative ω_h
k_{thp}	drag friction coefficient of the tail propeller for positive ω_h
k_{tvn}	drag friction coefficient of the main propeller for negative ω_v
k_{tvp}	drag friction coefficient of the main propeller for positive ω_v
l_b	length of the counterweight beam
l_{cb}	distance between the counterweight and the joint

$$J_{v5} = m_{tr} l_t^2 \tag{11}$$

$$J_{v6} = m_t l_t^2 \Big/ 3 \tag{12}$$

$$J_{v7} = m_{ms} r_{ms}^2 \Big/ 2 + m_{ms} l_m^2 \tag{13}$$

$$J_{v8} = m_{ts} r_{ts}^2 \Big/ 2 + m_{ts} l_t^2 \tag{14}$$

The non-linear functions $f_i(.)$, that take into account the frictions and coupling effects between the horizontal and the vertical dynamics, are defined as:

$$f_1(\omega_h) = \begin{cases} k_{thp}\omega_h^2 & \text{if} \quad \omega_h \geq 0 \\ -k_{thn}\omega_h^2 & \text{if} \quad \omega_h < 0 \end{cases} \tag{15}$$

$$f_2(\omega_h) = \begin{cases} k_{fhp}\omega_h^2 & \text{if} \quad \omega_h \geq 0 \\ -k_{fhn}\omega_h^2 & \text{if} \quad \omega_h < 0 \end{cases} \tag{16}$$

$$f_3(\theta_h) = \begin{cases} k_{chp}\theta_h & \text{if} \quad \theta_h \geq 0 \\ k_{chn}\theta_h & \text{if} \quad \theta_h < 0 \end{cases} \tag{17}$$

Table 4: TRMS parameters (part 3)

Symbol	Description
l_m	length of the main part of the beam
l_t	length of the tail part of the beam
m_b	mass of the counterweight beam
m_{cb}	mass of the counterweight
m_m	mass of the main part of the beam
m_{mr}	mass of the main DC motor
m_{ms}	mass of the main shield
m_t	mass of the tail part of the beam
m_{tr}	mass of the tail DC motor
m_{ts}	mass of the tail shield
R_a	armature resistance of the DC motors
r_{ms}	radius of the main shield
r_{ts}	radius of the tail shield
S_h	angular momentum of the TRMS in the horizontal plane
S_v	angular momentum of the TRMS in the vertical plane
u_h	input voltage of the tail motor
u_v	input voltage of the main motor
θ_h	yaw angle of the beam
θ_v	pitch angle of the beam
θ_v^0	equilibrium pitch angle corresponding to $u_v = 0$
ω_h	rotational velocity of the tail rotor
Ω_h	angular velocity of the TRMS around the vertical axis
ω_v	rotational velocity of the main rotor
Ω_v	angular velocity of the TRMS around the horizontal axis

$$f_4(\omega_v) = \begin{cases} k_{tvp}\omega_v^2 & \text{if} \quad \omega_v \geq 0 \\ -k_{tvn}\omega_v^2 & \text{if} \quad \omega_v < 0 \end{cases} \tag{18}$$

$$f_5(\omega_v) = \begin{cases} k_{fvp}\omega_v^2 & \text{if} \quad \omega_v \geq 0 \\ -k_{fvn}\omega_v^2 & \text{if} \quad \omega_v < 0 \end{cases} \tag{19}$$

$$f_6(\theta_v) = \begin{cases} k_{cvp}\left(\theta_v - \theta_v^0\right)^2 & \text{if } \theta_v \geqslant \theta_v^0 \\ k_{cvn}\left(\theta_v - \theta_v^0\right)^2 & \text{if } \theta_v < \theta_v^0 \end{cases} \tag{20}$$

where θ_v^0 is the equilibrium point for the vertical angle corresponding to $u_v = 0$. Finally, the constants of the non-linear model (1)-(6) are defined as:

$$K_A = (m_t/2 + m_{tr} + m_{ts})\, l_t \tag{21}$$

$$K_B = (m_m/2 + m_{mr} + m_{ms})\, l_m \tag{22}$$

$$K_C = (m_b l_b/2 + m_{cb} l_{cb}) \tag{23}$$

$$K_D = (m_m/3 + m_{mr} + m_{ms})\, l_m^2 + (m_t/3 + m_{tr} + m_{ts})\, l_t^2 \tag{24}$$

$$K_E = m_b l_b^2/3 + m_{cb} l_{cb}^2 \tag{25}$$

$$K_F = m_{ms} r_{ms}^2 + m_{ts} r_{ts}^2/2 \tag{26}$$

$$K_H = K_A l_t + K_B l_m + m_b l_b^2/2 + m_{cb} l_{cb} \tag{27}$$

For a complete description of the TRMS parameters, see Tables 2, 3 and 4.

3. Quasi-LPV Modeling of the TRMS

3.1. Quasi-LPV Systems

A quasi-LPV system is defined as a linear time-varying plant whose state-space matrices are functions of some varying parameters vector $\boldsymbol{\psi}(t)$ (continuous-time quasi-LPV system) or $\boldsymbol{\psi}(k)$ (discrete-time quasi-LPV system) that depends on the state variables. It can be described by continuous-time state-space equations of the form:

$$\dot{\boldsymbol{x}}(t) = \mathbf{A}\left(\boldsymbol{\psi}(t)\right)\boldsymbol{x}(t) + \mathbf{B}\left(\boldsymbol{\psi}(t)\right)\boldsymbol{u}(t) \tag{28}$$

$$\boldsymbol{y}(t) = \mathbf{C}\left(\boldsymbol{\psi}(t)\right)\boldsymbol{x}(t) + \mathbf{D}\left(\boldsymbol{\psi}(t)\right)\boldsymbol{u}(t) \tag{29}$$

or by discrete-time state-space equations of the form:

$$\boldsymbol{x}(k+1) = \mathbf{A}\left(\boldsymbol{\psi}(k)\right)\boldsymbol{x}(k) + \mathbf{B}\left(\boldsymbol{\psi}(k)\right)\boldsymbol{u}(k) \tag{30}$$

$$\boldsymbol{y}(k) = \mathbf{C}\left(\boldsymbol{\psi}(k)\right)\boldsymbol{x}(k) + \mathbf{D}\left(\boldsymbol{\psi}(k)\right)\boldsymbol{u}(k) \tag{31}$$

where $\mathbf{A}(\boldsymbol{\psi}(.)) \in \mathbb{R}^{n_x \times n_x}$, $\mathbf{B}(\boldsymbol{\psi}(.)) \in \mathbb{R}^{n_x \times n_u}$ and $\mathbf{C}(\boldsymbol{\psi}(.)) \in \mathbb{R}^{n_y \times n_x}$ are time-varying matrices scheduled by $\boldsymbol{\psi}(.)$, the vector of varying parameters that depends on some system variables $\boldsymbol{p}(.)$ that can be estimated using some function $\boldsymbol{\psi}(.) = \boldsymbol{f}_{\psi}(\boldsymbol{p}(.))$, known as *scheduling function*.

In this paper, the particular class of LPV systems that are strictly proper, that is, $\mathbf{D}(\boldsymbol{\psi}(.)) = \mathbf{0}$, and whose input and output matrices are invariant, that is, $\mathbf{B}(\boldsymbol{\psi}(.)) = \mathbf{B}$ and $\mathbf{C}(\boldsymbol{\psi}(.)) = \mathbf{C}$, is considered.

3.2. Automated Generation of LPV Models

An LPV system is called *polytopic* if the state-space model depends on the parameters in a polytopic manner, i.e. if:

$$\mathbf{A}(\boldsymbol{\psi}(.)) = \sum_{i=1}^{N} \pi_i(\boldsymbol{\psi}(.))\mathbf{A}_i \tag{32}$$

with $\sum_{i=1}^{N} \pi_i(.) = 1$ and $\pi_i(.) \geq 0$ for $i = 1, \ldots, N$. Kwiatkowski et al. (2006) presented a method for automated generation of LPV polytopic models, generated from general nonlinear models by "hiding" the nonlinearities inside the scheduling parameters. The method facilitates the construction of a suitable LPV model from a given non-linear system:

$$\dot{\boldsymbol{x}}(t) = \boldsymbol{f}(\boldsymbol{x}(t), \boldsymbol{u}(t)) \tag{33}$$

$$\boldsymbol{y}(t) = \boldsymbol{g}(\boldsymbol{x}(t), \boldsymbol{u}(t)) \tag{34}$$

In order to generate LPV models automatically, the model (33)-(34) must be converted into a suitable form. This is done by expanding each row of (33)-(34) into its summands:

$$\dot{x}_i = \sum_{j=1}^{r_{x_i}} f_{ij}(\boldsymbol{x}, \boldsymbol{u}) \quad , \quad i = 1, \ldots, n_x \tag{35}$$

$$y_i = \sum_{j=1}^{r_{y_i}} g_{ij}(\boldsymbol{x}, \boldsymbol{u}) \quad , \quad i = 1, \ldots, n_y \tag{36}$$

where the integers r_{x_i} and r_{y_i} denote the number of summands in each row of the state equation (33) and the output equation (34), respectively. Since there is no difference in handling a state or output equation, only the state equation will be considered in the following.

Each term is decomposed into its numerator n_{ij}, denominator d_{ij} and a constant factor k_{ij}:

$$\dot{x}_i = \sum_{j=1}^{r_{x_i}} k_{ij} \frac{n_{ij}(\boldsymbol{x}, \boldsymbol{u})}{d_{ij}(\boldsymbol{x}, \boldsymbol{u})} \quad , \quad i = 1, \ldots, n_x \tag{37}$$

The numerator is factored to determine the possibilities of "hiding" the nonlinearities in the parameters:

$$n_{ij} = \prod_{q=1}^{n_x} \prod_{r=1}^{n_u} h_{ij}(\boldsymbol{x}, \boldsymbol{u}) x_q^{\mu_q} u_r^{\nu_r} \tag{38}$$

where $h_{ij}(\boldsymbol{x}, \boldsymbol{u})$ denotes a "non-factorizable" term, $\mu_q \in \mathbb{Z}^+$ and $\nu_r \in \mathbb{Z}^+$ are the integer power of the state x_q and input u_r, respectively. The classification of a term is determined by the structure of its numerator. Two classes can be distinguished:

- *Constant or non-factorizable numerator,* $\mathcal{K}_0$: for a term of this class a factor of the state $x_q^{\mu_q}$ or input $u_r^{\nu_r}$ as an element of the system matrix could not be chosen;
- *Arbitrary positive power of factor,* $\mathcal{K}_p$: this class consists of terms that have numerators with positive integer powers of a state variable $x_q^{\mu_q}$ or input $u_r^{\nu_r}$.

According to this term classification, parameter components ϑ_{ij} can be chosen as follows:

$$\vartheta_{ij}^a = k_{ij} \frac{n_{ij}(\boldsymbol{x}, \boldsymbol{u})}{d_{ij} x_l} \quad , \quad l = 1, \ldots, n_x \tag{39}$$

$$\vartheta_{ij}^b = k_{ij} \frac{n_{ij}(\boldsymbol{x}, \boldsymbol{u})}{d_{ij} u_l} \quad , \quad l = 1, \ldots, n_u \tag{40}$$

where if the numerator is $\mathcal{K}_0$, the parameter can be taken using n_x possible assignments to the system matrix $\mathbf{A}$ and n_u possible assignments to the input matrix $\mathbf{B}$. If the numerator is $\mathcal{K}_p$ the parameter is a factor of the numerator.

In the final step, the matrix elements a_{ij} and b_{ij} and the corresponding parameters $\boldsymbol{\psi}$ need to be derived from the parameter components ϑ_{ij}^a and ϑ_{ij}^b. Hereafter, the state space matrix is given by *superposition*, where all contributions of a summand to a state space matrix element are superimposed and a_{ij} becomes an element of the vector $\boldsymbol{\psi}$.

3.3. Quasi-LPV Absolute Representation of the TRMS

The non-linear model (1)-(6) can be expressed in the quasi-LPV absolute form following the parameter non-linear embedding approach proposed in (Kwiatkowski

et al., 2006)[1]:

$$\begin{bmatrix} \dot{\omega}_h(t) \\ \dot{\Omega}_h(t) \\ \dot{\theta}_h(t) \\ \dot{\omega}_v(t) \\ \dot{\Omega}_v(t) \\ \dot{\theta}_v(t) \end{bmatrix} = \mathbf{A}(\boldsymbol{\psi}(t)) \begin{bmatrix} \omega_h(t) \\ \Omega_h(t) \\ \theta_h(t) \\ \omega_v(t) \\ \Omega_v(t) \\ \theta_v(t) - \theta_v^0 \end{bmatrix} + \begin{bmatrix} b_{11} & 0 \\ 0 & b_{22}(\boldsymbol{p}(t)) \\ 0 & 0 \\ 0 & b_{42} \\ b_{51} & 0 \\ 0 & 0 \end{bmatrix} \begin{bmatrix} u_h(t) \\ u_v(t) \end{bmatrix} \tag{41}$$

where $\boldsymbol{\psi}(t) = [a_{11}, a_{21}, a_{22}, a_{23}, a_{24}, a_{25}, a_{26}, a_{44}, a_{52}, a_{54}, a_{56}]^T$ is the vector of varying parameters scheduled by $\boldsymbol{p}(t) = [\theta_h(t), \theta_v(t), \omega_h(t), \omega_v(t), \Omega_h(t)]^T$. Notice that the vector $\boldsymbol{p}(t)$ does not contain the state Ω_v as this state variable does not affect the values of the elements in the model (41).

The matrix $\mathbf{A}(\boldsymbol{\psi}(t))$ is defined as:

$$A(\boldsymbol{\psi}(t)) = \begin{bmatrix} \psi_1(\boldsymbol{p}(t)) & 0 & 0 & 0 & 0 & 0 \\ \psi_2(\boldsymbol{p}(t)) & \psi_3(\boldsymbol{p}(t)) & \psi_4(\boldsymbol{p}(t)) & \psi_5(\boldsymbol{p}(t)) & \psi_6(\boldsymbol{p}(t)) & \psi_7(\boldsymbol{p}(t)) \\ 0 & 1 & 0 & 0 & 0 & 0 \\ 0 & 0 & 0 & \psi_8(\boldsymbol{p}(t)) & 0 & 0 \\ \frac{k_t}{J_v}\psi_1(\boldsymbol{p}(t)) & \psi_9(\boldsymbol{p}(t)) & 0 & \psi_{10}(\boldsymbol{p}(t)) & a_{55} & \psi_{11}(\boldsymbol{p}(t)) \\ 0 & 0 & 0 & 0 & 1 & 0 \end{bmatrix} \tag{42}$$

with:

$$\psi_1(\boldsymbol{p}(t)) = a_{11}(\boldsymbol{p}(t)) = -\frac{k_a^2/R_a + B_{tr} + f_1(\omega_h)/\omega_h}{J_{tr}} \tag{43}$$

$$\psi_2(\boldsymbol{p}(t)) = a_{21}(\boldsymbol{p}(t)) = \frac{l_t \cos\theta_v f_2(\omega_h)/\omega_h}{K_D \cos^2\theta_v + K_E \sin^2\theta_v + K_F} \tag{44}$$

$$\psi_3(\boldsymbol{p}(t)) = a_{22}(\boldsymbol{p}(t)) = -\frac{k_{oh}}{K_D \cos^2\theta_v + K_E \sin^2\theta_v + K_F} \tag{45}$$

$$\psi_4(\boldsymbol{p}(t)) = a_{23}(\boldsymbol{p}(t)) = -\frac{f_3(\theta_h)/\theta_h}{K_D \cos^2\theta_v + K_E \sin^2\theta_v + K_F} \tag{46}$$

$$\psi_5(\boldsymbol{p}(t)) = a_{24}(\boldsymbol{p}(t)) = -\frac{k_m\left(k_a^2/R_a + B_{mr} + f_4(\omega_v)/\omega_v\right)\cos\theta_v}{\left(K_D \cos^2\theta_v + K_E \sin^2\theta_v + K_F\right) J_{mr}} \tag{47}$$

[1]The input matrix $\mathbf{B}$ is not invariant. However, after the system identification phase, it has been noticed that the range of variation of the element $b_{22}(\boldsymbol{p}(k))$ is small enough to allow its approximation with a constant value.

$$\psi_6(\boldsymbol{p}(t)) = a_{25}(\boldsymbol{p}(t)) = \frac{k_m \omega_v \sin\theta_v \left(K_D \cos^2\theta_v - K_E \sin^2\theta_v - K_F - 2K_E \cos^2\theta_v\right)}{\left(K_D \cos^2\theta_v + K_E \sin^2\theta_v + K_F\right)^2} \tag{48}$$

$$\psi_7(\boldsymbol{p}(t)) = a_{26}(\boldsymbol{p}(t)) = \frac{f_6(\theta_v)/(\theta_v - \theta_v^0)}{K_D \cos^2\theta_v + K_E \sin^2\theta_v + K_F} \tag{49}$$

$$\psi_8(\boldsymbol{p}(t)) = a_{44}(\boldsymbol{p}(t)) = -\frac{k_a^2/R_a + B_{mr} + f_4(\omega_v)/\omega_v}{J_{mr}} \tag{50}$$

$$\psi_9(\boldsymbol{p}(t)) = a_{52}(\boldsymbol{p}(t)) = \frac{k_g \cos\theta_v f_5(\omega_v) - \Omega_h K_H \sin\theta_v \cos\theta_v}{J_v} \tag{51}$$

$$\psi_{10}(\boldsymbol{p}(t)) = a_{54}(\boldsymbol{p}(t)) = \frac{l_m f_5(\omega_v)/\omega_v}{J_v} \tag{52}$$

$$a_{55} = -\frac{k_{ov}}{J_v} \tag{53}$$

$$\psi_{11}(\boldsymbol{p}(t)) = a_{56}(\boldsymbol{p}(t)) = \frac{g\left((K_A - K_B)\cos\theta_v - K_C \sin\theta_v\right)}{J_v(\theta_v - \theta_v^0)} \tag{54}$$

$$b_{11} = \frac{k_a k_1}{J_{tr} R_a} \tag{55}$$

$$b_{22}(\boldsymbol{p}(t)) = \frac{k_m \cos(\theta_v) k_a k_2}{(K_D \cos^2\theta_v + K_E \sin^2\theta_v + K_F) R_a J_{mr}} \tag{56}$$

$$b_{42} = \frac{k_a k_2}{J_{mr} R_a} \tag{57}$$

$$b_{51} = \frac{k_a k_1 k_t}{J_v J_{tr} R_a} \tag{58}$$

A discrete-time quasi-LPV model can be obtained using Euler approximation with a sample time T_s to allow a digital implementation of the observer/controller:

$$\begin{bmatrix} \omega_h(k+1) \\ \Omega_h(k+1) \\ \theta_h(k+1) \\ \omega_v(k+1) \\ \Omega_v(k+1) \\ \theta_v(k+1) \end{bmatrix} = \mathbf{A_d}(\boldsymbol{\psi_d}(k)) \begin{bmatrix} \omega_h(k) \\ \Omega_h(k) \\ \theta_h(k) \\ \omega_v(k) \\ \Omega_v(k) \\ \theta_v(k) - \theta_v^0 \end{bmatrix} + \mathbf{B_d}(\mathbf{p_d}(k)) \begin{bmatrix} u_h(k) \\ u_v(k) \end{bmatrix} \tag{59}$$

$$\mathbf{A_d}(\boldsymbol{\psi_d}(k)) = \begin{bmatrix} \psi_{1d} & 0 & 0 & 0 & 0 & 0 \\ \psi_{2d} & \psi_{3d} & \psi_{4d} & \psi_{5d} & \psi_{6d} & \psi_{7d} \\ 0 & T_s & 1 & 0 & 0 & 0 \\ 0 & 0 & 0 & \psi_{8d} & 0 & 0 \\ \frac{k_t}{J_v}(\psi_{1d} - 1) & \psi_{9d} & 0 & \psi_{10d} & 1 + a_{55}T_s & \psi_{11d} \\ 0 & 0 & 0 & 0 & 1 & 0 \end{bmatrix} \tag{60}$$

$$\mathbf{B_d}(\boldsymbol{p_d}(k)) = \begin{bmatrix} b_{11}T_s & 0 \\ 0 & b_{22}T_s \\ 0 & 0 \\ 0 & b_{42}T_s \\ b_{51}T_s & 0 \\ 0 & 0 \end{bmatrix} \tag{61}$$

with $\psi_{1d} = 1 + a_{11}T_s$, $\psi_{2d} = a_{21}T_s$, $\psi_{3d} = 1 + a_{22}T_s$, $\psi_{4d} = a_{23}T_s$, $\psi_{5d} = a_{24}T_s$, $\psi_{6d} = a_{25}T_s$, $\psi_{7d} = a_{26}T_s$, $\psi_{8d} = 1 + a_{44}T_s$, $\psi_{9d} = a_{52}T_s$, $\psi_{10d} = a_{54}T_s$, $\psi_{11d} = a_{56}T_s$, where the dependence of the elements of the matrices on $\boldsymbol{p_d}(k)$ has been omitted.

3.4. Generation of Polytopic LPV Models

In (Apkarian et al., 1995) and (Chilali & Gahinet, 1996), linear matrix inequality techniques are applied for gain-scheduled control of LPV systems. The suggested method possesses a strong form of robust stability with respect to time-varying parameters and exploits the realness of the parameters, producing a less conservative design than the one in the Linear Fractional Transformation form (Packard, 1994). However, a limitation in the use of this synthesis approach lies in the fact that it is generally associated with a convex feasibility problem with infinite constraints imposed on an LMI formulation. One effective way to solve this problem is reducing the LMI constraints to a finite number through affine LPV modeling.

Sun & Postlethwaite (1998) describe a practical technique for modeling affine LPV systems, starting with the basic assumption that measurements of $\boldsymbol{\psi}$ are available in real-time and the range of the elements of $\boldsymbol{\psi}$ is known a priori:

$$\underline{\psi}_j \leq \psi_j \leq \overline{\psi}_j \tag{62}$$

where $\underline{\psi}_j$ and $\overline{\psi}_j$ are lower and upper bounds of each element.

Vectors $\boldsymbol{\omega}_i$ can be formed by taking each possible permutation of upper and lower bounds of elements in $\boldsymbol{\psi}$. There will be $N = 2^{n_\psi}$ vectors $\boldsymbol{\omega}_i$ such that the

parameter vector $\boldsymbol{\psi}$ can be put into polytopic form:

$$\boldsymbol{\psi} \in Co\left\{\boldsymbol{\omega}_1, \boldsymbol{\omega}_2, \ldots, \boldsymbol{\omega}_N\right\} := \left\{ \sum_{i=1}^{N} \pi_i \boldsymbol{\omega}_i : \pi_i \geq 0, \sum_{i=1}^{N} \pi_i = 1 \right\} \tag{63}$$

meaning that the vector $\boldsymbol{\psi}$ belongs to the convex hull formed by the vertices $\boldsymbol{\omega}_i$. This modeling approach is referred to as *bounding box method* because the convex hull generated by such approach always has the shape of a rectangular bounding box, that is, a hyperrectangle.

If an affine function $\boldsymbol{\delta}(\boldsymbol{\psi})$ is applied to the vector $\boldsymbol{\psi}$, the result can be put into a polytopic form:

$$\boldsymbol{\delta}(\boldsymbol{\psi}) \in Co\left\{\boldsymbol{\delta}(\boldsymbol{\omega}_1), \ldots, \boldsymbol{\delta}(\boldsymbol{\omega}_N)\right\} := \left\{ \sum_{i=1}^{N} \pi_i \boldsymbol{\delta}(\boldsymbol{\omega}_i) : \pi_i \geq 0, \sum_{i=1}^{N} \pi_i = 1 \right\} \tag{64}$$

Thus, if the state matrix of the LPV system $\mathbf{A}(\boldsymbol{\psi})$ depends affinely on $\boldsymbol{\psi}$, it will range in a polytope of matrices whose vertices are the images of the vertices $\boldsymbol{\omega}_i$:

$$\mathbf{A}(\boldsymbol{\psi}(k)) \in Co\left\{\mathbf{A}_i, i = 1, \ldots, N\right\} := \sum_{i=1}^{N} \pi_i(\boldsymbol{\psi}(k))\mathbf{A}_i \tag{65}$$

with $\pi_i\left(\boldsymbol{\psi}(k)\right) \geq 0$ and $\sum_{i=1}^{N} \pi_i\left(\boldsymbol{\psi}(k)\right) = 1$, where each i^{th} model is called a *vertex* system. Because of this property, such LPV systems are referred to as *polytopic*.

3.5. Quasi-LPV Polytopic Representation of the TRMS

To obtain the quasi-LPV polytopic representation of the TRMS, the *bounding box method* is applied to the TRMS absolute discrete-time representation (59)-(61). Each element of the vector $\boldsymbol{p}(k) = [\theta_h(k), \theta_v(k), \omega_h(k), \omega_v(k), \Omega_h(k)]^T$ is assumed to take values in an interval known a priori (e.g. $\theta_h \in \left[\underline{\theta}_h, \overline{\theta}_h\right]$). Then, for each of the scheduling parameters in the vector $\boldsymbol{\psi}(k)$, its minimum and maximum values over the allowed values of the elements of $\boldsymbol{p}(k)$ are calculated. For example, consider the discrete-time $\psi_{1d}(\boldsymbol{p}(k))$:

$$\psi_{1d}(\boldsymbol{p}(k)) = \begin{cases} 1 - \frac{T_s}{J_{tr}}\left(\frac{k_a^2}{R_a} + B_{tr} + k_{thp}\omega_h\right) & if\ \omega_h \geq 0 \\ 1 - \frac{T_s}{J_{tr}}\left(\frac{k_a^2}{R_a} + B_{tr} - k_{thn}\omega_h\right) & if\ \omega_h < 0 \end{cases} \tag{66}$$

In this case, the extreme values $\underline{\psi}_{1d}$ and $\overline{\psi}_{1d}$ are given by:

$$\underline{\psi}_{1d} = 1 - \frac{T_s}{J_{tr}}\left(\frac{k_a^2}{R_a} + B_{tr} + \max\left\{k_{thp}\overline{\omega}_h, -k_{thn}\underline{\omega}_h\right\}\right) \tag{67}$$

$$\overline{\psi}_{1d} = 1 - \frac{T_s}{J_{tr}}\left(\frac{k_a^2}{R_a} + B_{tr}\right) \tag{68}$$

When each of the scheduling parameters takes an extreme value, one of the vertex systems in (65) is generated.

The strong nonlinearity of some of the scheduling parameters makes hard to obtain an analytic expression so as to find the exact optima over the entire range of values that the elements of $\boldsymbol{p}(k)$ can take. In these cases, approximate optima have to be found by means of numerical optimization methods. It should also be considered that some LPV parameters are not defined when $\omega_h = 0$, and that they take very high values when ω_h is near zero, so an additional limit on ω_h will be imposed:

$$\omega_h \in [\underline{\omega}_h, \omega_h^-] \cup [\omega_h^+, \overline{\omega}_h] \tag{69}$$

where ω_h^- and ω_h^+ are values near to 0. The same is true for ω_v and θ_h near zero and θ_v near θ_v^0, leading to analogous additional limits on these variables.

The values of the parameters appearing in the elements of the matrix $\mathbf{A}$ in (41) must be known in order to calculate the vertex systems for control design purposes. Some of these values are given by the manufacturer while others need to be estimated. This leads to the necessity of performing system identification.

4. Identification of the TRMS

In this section, the identification procedure to estimate the unknown parameters of the TRMS is presented (see Table 5 for the list of known and unknown parameters). At first, the unknown parameters of motor-propellers are identified. Then, those of the aerodynamical part are estimated. The spirit of the method is to compare, at each step, the data obtained from the real set-up with the data obtained by simulating part of the TRMS continuous-time non-linear model. This is included in an optimization problem so as to find the parameter values that give simulation results that better approximate the real system. The values estimated for the model parameters will be used to obtain the TRMS quasi-LPV model. From the LPV identification point of view, the method described hereafter can be considered as a *glocal* approach, because the global LPV model is estimated from local experiments (Mercere et al., 2011).

4.1. Tail and Main Propeller

The identification procedure is based on the knowledge of the non-linear model of the tail (1) and main (4) propellers. The goal is to identify J_{tr}, B_{tr}, k_{thp} and k_{thn}

Table 5: Known and unknown parameters

Parameter	Value	Parameter	Value	Parameter	Value
k_g	0.2	$L_{ah/av}$	0.86e-3	m_t	0.015
l_t	0.282	$k_{ah/av}$	0.0202	m_{tr}	0.221
l_m	0.246	B_{tr}	unknown	m_{ts}	0.119
l_b	0.290	B_{mr}	unknown	J_{tr}	unknown
l_{cb}	0.276	$k_{thp/n}$	unknown	J_{mr}	unknown
r_{ts}	0.1	$k_{tvp/n}$	unknown	$R_{ah/av}$	8
r_{ms}	0.155	k_{fhp}	unknown	k_t	unknown
m_{cb}	0.068	k_{fhn}	unknown	k_m	unknown
m_b	0.022	k_{fvp}	unknown	k_1	6.5
m_m	0.014	k_{fvn}	unknown	k_2	8.5
m_{mr}	0.236	k_{chp}	unknown	k_{oh}	unknown
m_{ms}	0.219	k_{chn}	unknown	k_{ov}	unknown
		k_{cvp}	unknown	k_{cvn}	unknown

for the tail propeller and J_{mr}, B_{mr}, k_{tvp} and k_{tvn} for the main propeller. The rest of parameters are assumed to be known, as their values are given by the manufacturer. The identification procedure should identify some values for the unknown parameters in such a manner that the non-linear model behavior resembles the real behavior of the tail and main propellers.

It is assumed to have at disposal $N_{\omega h}$ sets of data $\left\{u_h^i(k) - \omega_h^i(k)\right\}$ for the tail propeller, where $i = 1, \ldots, N_{\omega_h}$ and $k = 1, \ldots, K_{\omega h}^i$ with $K_{\omega h}^i$ being the number of samples of the i^{th} set of data, and $N_{\omega v}$ sets of data $\left\{u_v^i(k) - \omega_v^i(k)\right\}$ for the main propeller, with $i = 1, \ldots, N_{\omega_v}$ and $k = 1, \ldots, K_{\omega v}^i$.

The identification procedure finds the minimum of the following objective functions over the unknown parameters:

$$\min_{J_{tr}, B_{tr}, k_{thp}, k_{thn}} J_{\omega h} = \sum_{i=1}^{N_{\omega h}} \sum_{k=1}^{K_{\omega h}^i} \left(\omega_h^i(k) - \hat{\omega}_h^i(k)\right)^2 \tag{70}$$

$$\min_{J_{mr}, B_{mr}, k_{tvp}, k_{tvn}} J_{\omega v} = \sum_{i=1}^{N_{\omega v}} \sum_{k=1}^{K_{\omega v}^i} \left(\omega_v^i(k) - \hat{\omega}_v^i(k)\right)^2 \tag{71}$$

where $\hat{\omega}_h^i(k)$ and $\hat{\omega}_v^i(k)$ are the one-step predictions based on the non-linear equations (1) and (4). Notice that, while all the sets of data can be used to identify J_{tr},

J_{mr}, B_{tr} and B_{mr}, a numerical value of k_{thp} and k_{tvp} can be obtained only from those sets of data where the input voltage u_h or u_v is positive. Analogously, a numerical value of k_{thn} and k_{tvn} can be obtained only from those sets of data where the input voltage u_h or u_v is negative.

4.2. Tail Propeller to Horizontal Aeromechanics

The identification procedure is based on the knowledge of the non-linear model (2)-(3). In this step, the horizontal dynamics due to an input voltage acting on the tail propeller are identified (unknown parameters: k_{fhp}, k_{fhn}, k_{oh}, k_{chp}, k_{chn}).

When no input voltage acts on the main propeller, (2) and (3) simplify to:

$$\frac{d\Omega_h}{dt} = \frac{l_t f_2(\omega_h)\cos\theta_v^0 - k_{oh}\Omega_h - f_3(\theta_h)}{K_D\cos^2\theta_v^0 + K_E\sin^2\theta_v^0 + K_F} \tag{72}$$

$$\frac{d\theta_h}{dt} = \Omega_h \tag{73}$$

Replacing (73) in (72) and using Laplace transform leads to:

$$\Theta_h(s) = \frac{K_p}{1 + 2\xi_p T_p s + (T_p)^2 s^2}\Psi_h(s) \quad if\ \omega_h \geq 0 \tag{74}$$

$$\Theta_h(s) = \frac{K_n}{1 + 2\xi_n T_n s + (T_n)^2 s^2}\Psi_h(s) \quad if\ \omega_h < 0 \tag{75}$$

where $\Theta_h(s)$ is the Laplace transform of $\theta_h(t)$, $\Psi_h(s)$ is the Laplace transform of $\omega_h^2(t)$ and:

$$K_p = (l_t k_{fhp}\cos\theta_v^0)/k_{chp} \tag{76}$$

$$K_n = -(l_t k_{fhn}\cos\theta_v^0)/k_{chn} \tag{77}$$

$$2\xi_p T_p = k_{oh}/k_{chp} \tag{78}$$

$$2\xi_n T_n = k_{oh}/k_{chn} \tag{79}$$

$$T_p^2 = (K_D\cos^2\theta_v^0 + K_E\sin^2\theta_v^0 + K_F)/k_{chp} \tag{80}$$

$$T_n^2 = (K_D\cos^2\theta_v^0 + K_E\sin^2\theta_v^0 + K_F)/k_{chn} \tag{81}$$

Hence, the knowledge of K_p, K_n, ξ_p, ξ_n, T_p and T_n can be used for the estimation of the unknown parameters:

$$k_{chp} = (K_D\cos^2\theta_v^0 + K_E\sin^2\theta_v^0 + K_F)/T_p^2 \tag{82}$$

$$k_{chn} = (K_D \cos^2 \theta_v^0 + K_E \sin^2 \theta_v^0 + K_F)/T_n^2 \tag{83}$$

$$k_{oh} = \begin{cases} 2\xi_p T_p k_{chp} \\ 2\xi_n T_n k_{chn} \end{cases} \tag{84}$$

$$k_{fhp} = K_p k_{chp}/(l_t \cos \theta_v^0) \tag{85}$$

$$k_{fhn} = -K_n k_{chn}/(l_t \cos \theta_v^0) \tag{86}$$

Values of K_p and K_n can be found in a simple way through the knowledge of the steady-state values of ω_h and θ_h:

$$K_p = \theta_h^\infty/(\omega_h^\infty)^2 \quad with\ \omega_h^\infty, \theta_h^\infty > 0 \tag{87}$$

$$K_n = \theta_h^\infty/(\omega_h^\infty)^2 \quad with\ \omega_h^\infty, \theta_h^\infty < 0 \tag{88}$$

Values of T_p, T_n , ξ_p and ξ_n can be estimated by means of some well-known second-order system identification method (Ljung, 1997). It is assumed to have at disposal sets of data corresponding to the response of the horizontal aeromechanical subsystem to a step input voltage in the tail motor. By applying the described procedure to each set of data, different values for the unknown parameters can be obtained. Such values can be used to define lower bounds and upper bounds for the values of the unknown parameters (e.g. $\underline{k}_{fhp}$ and $\overline{k}_{fhp}$).

Afterwards, another identification stage can be performed. In this stage, it is assumed to have at disposal N_{hh} sets of data $\left\{\omega_h^i(k), \theta_h^i(k)\right\}$ where $i = 1, \ldots, N_{hh}$, $k = 1, \ldots, K_i$ and K_i is the number of samples of the i-th set of data. The minimum of the objective function J_{hh} over the unknown parameters k_{fhp}, k_{fhn}, k_{oh}, k_{chp} and k_{chn}:

$$\begin{gathered} \min \\ k_{fhp} \in [\underline{k}_{fhp}, \overline{k}_{fhp}] \\ k_{fhn} \in [\underline{k}_{fhn}, \overline{k}_{fhn}] \\ k_{oh} \in [\underline{k}_{oh}, \overline{k}_{oh}] \\ k_{chp} \in [\underline{k}_{chp}, \overline{k}_{chp}] \\ k_{chn} \in [\underline{k}_{chn}, \overline{k}_{chn}] \end{gathered} \quad J_{hh} = \sum_{i=1}^{N_{hh}} \sum_{k=1}^{K_i} \left(\theta_h^i(k) - \hat{\theta}_h^i(k)\right)^2 \tag{89}$$

should be found, where $\hat{\theta}_h^i(k)$ is the one-step prediction based on the non-linear model (72)-(73), obtained by considering that both ω_h and θ_v are provided by the sensors.

4.3. Main Propeller to Horizontal Aeromechanics

In this step, the horizontal dynamics due to an input voltage acting on the main propeller are identified (unknown parameters: k_m, k_{cvp}, k_{cvn}). When no input voltage acts on the tail propeller, (2) and (3) simplify to:

$$\begin{aligned}\frac{d\Omega_h}{dt} &= \frac{k_m\omega_v \sin\theta_v\Omega_v\left(K_D\cos^2\theta_v - K_E\sin^2\theta_v - K_F - 2K_E\cos^2\theta_v\right)}{\left(K_D\cos^2\theta_v + K_E\sin^2\theta_v + K_F\right)^2} \\ &+\frac{-k_{oh}\Omega_h - f_3(\theta_h) + f_6(\theta_v)}{K_D\cos^2\theta_v + K_E\sin^2\theta_v + K_F} \\ &+\frac{k_m\cos\theta_v\left(\frac{k_ak_2}{R_a}u_v - \left(B_{mr} + \frac{k_a^2}{R_a}\right)\omega_v - f_4(\omega_v)\right)}{J_{mr}\left(K_D\cos^2\theta_v + K_E\sin^2\theta_v + K_F\right)} \end{aligned} \tag{90}$$

$$\frac{d\theta_h}{dt} = \Omega_h \tag{91}$$

It is assumed to have at disposal N_{vh} sets of data $\left\{\omega_v^i(k), \theta_v^i(k), \theta_h^i(k)\right\}$ where $i = 1,\ldots,N_{vh}$, $k = 1,\ldots,K_i$ with K_i being the number of samples of the i-th set of data. The identification procedure should identify values for k_m, k_{cvp} and k_{cvn}, as all other parameter values are given by the manufacturer or have been identified previously. If the input voltage in the main propeller is a step signal, at steady-state:

$$\Omega_v^\infty = \Omega_h^\infty = \frac{k_ak_2}{R_a}u_v - \left(B_{mr} + \frac{k_a^2}{R_a}\right)\omega_v - f_4(\omega_v) = 0 \tag{92}$$

and (90) reduces to:

$$\begin{cases} -k_{chp}\theta_h^\infty + k_{cvp}\left(\theta_v^\infty - \theta_v^0\right)^2 = 0 & if\ \theta_v \geq \theta_v^0 \\ -k_{chp}\theta_h^\infty + k_{cvn}\left(\theta_v^\infty - \theta_v^0\right)^2 = 0 & if\ \theta_v < \theta_v^0 \end{cases} \tag{93}$$

A first estimation of k_{cvp} and k_{cvn} can be obtained from (93) as:

$$k_{cvp} = k_{cvn} = \frac{k_{chp}\theta_h^\infty}{\left(\theta_v^\infty - \theta_v^0\right)^2} \tag{94}$$

Such estimation is used to define lower and upper bounds on the values of the unknown parameters. Later, k_m, k_{cvp} and k_{cvn} can be refined by solving the following

optimization problem:

$$\begin{array}{c}\min \\ k_{cvp} \in [\underline{k}_{cvp}, \overline{k}_{cvp}] \\ k_{cvn} \in [\underline{k}_{cvn}, \overline{k}_{cvn}] \\ k_m \in [\underline{k}_m, \overline{k}_m]\end{array} \quad J_{vh} = \sum_{i=1}^{N_{vh}} \sum_{k=1}^{K_i} \left(\theta_h^i(k) - \hat{\theta}_h^i(k)\right)^2 \tag{95}$$

where $\hat{\theta}_h^i(k)$ is the one-step prediction based on the non-linear model (90)-(91), obtained by considering that ω_v and θ_v are data provided by the sensors and that Ω_v can be obtained from θ_v by differentiation.

4.4. Main Propeller to Vertical Aeromechanics

In this step, the vertical dynamics due to an input voltage acting on the main propeller are identified (unknown parameters: k_m, k_{cvp}, k_{cvn}). When no input voltage acts on the tail propeller, (5) and (6) simplify to:

$$\begin{aligned}\frac{d\Omega_v}{dt} &= \frac{l_m f_5(\omega_v) + k_g \Omega_h f_5(\omega_v)\cos\theta_v - k_{ov}\Omega_v}{J_v} \\ &\quad \frac{-0.5\Omega_h^2 H \sin 2\theta_v + g\left((K_A - K_B)\cos\theta_v - K_C \sin\theta_v\right)}{J_v}\end{aligned} \tag{96}$$

$$\frac{d\theta_v}{dt} = \Omega_v \tag{97}$$

At steady-state, as $\Omega_h^\infty = 0$ and $\Omega_v^\infty = 0$:

$$\frac{l_m f_5(\omega_v^\infty) + g\left((K_A - K_B)\cos\theta_v^\infty - K_C \sin\theta_v^\infty\right)}{J_v} = 0 \tag{98}$$

Thus, a preliminary estimation of k_{fvp} and k_{fvn} can be obtained as:

$$k_{fvp} = \frac{g\left((K_B - K_A)\cos\theta_v^\infty + K_C \sin\theta_v^\infty\right)}{l_m\left(\omega_v^\infty\right)^2} \tag{99}$$

$$k_{fvn} = -\frac{g\left((K_B - K_A)\cos\theta_v^\infty + K_C \sin\theta_v^\infty\right)}{l_m\left(\omega_v^\infty\right)^2} \tag{100}$$

Analogously to the previous cases, these estimations are used to define lower and upper bounds on the values of the unknown parameters, whose values can be

refined by solving the optimization problem:

$$\begin{array}{c}\min \\ k_{fvp} \in [\underline{k}_{fvp}, \overline{k}_{fvp}] \\ k_{fvn} \in [\underline{k}_{fvn}, \overline{k}_{fvn}] \\ k_{ov} \in [\underline{k}_{ov}, \overline{k}_{ov}]\end{array} \quad J_{vv} = \sum_{i=1}^{N_{vv}} \sum_{k=1}^{K_i} \left(\theta_v^i(k) - \hat{\theta}_v^i(k)\right)^2 \tag{101}$$

where $\hat{\theta}_v^i(k)$ is the one-step prediction based on the non-linear model (96)-(97), obtained considering that ω_v is provided by the sensor, as well as θ_h that is used to obtain Ω_h by differentiation.

4.5. Tail Propeller to Vertical Aeromechanics

It has been noticed experimentally that when the main propeller is off, the TRMS remains in its equilibrium vertical angle θ_v^0 for each value of u_h. This suggests that $k_t = 0$ is a good approximation of the real value of this constant.

5. Control of the TRMS

The quasi-LPV system is controlled by a state feedback controller with tracking reference input as proposed in (Franklin et al., 1997). The control law can be expressed as follows:

$$\boldsymbol{u}(k) = \boldsymbol{u_r}(k) + \mathbf{K_d}(\boldsymbol{\psi}(k))(\hat{\boldsymbol{x}}(k) - \boldsymbol{x_r}(k)) \tag{102}$$

where the state reference $\boldsymbol{x_r}(k) \in \mathbb{R}^{n_x}$ and the feedforward control action $\boldsymbol{u_r}(k) \in \mathbb{R}^{n_u}$ correspond to an equilibrium point for the reference $\boldsymbol{r}(k)$. The matrix $\mathbf{K_d}(\boldsymbol{\psi}(k)) \in \mathbb{R}^{n_u \times n_x}$ is the gain of the LPV controller.

Notice that the estimated state $\hat{\boldsymbol{x}}(k)$ is used because $\boldsymbol{x}(k)$ is assumed not to be available. Consequently, an LPV state observer is used to provide such state estimation:

$$\hat{\boldsymbol{x}}(k+1) = \mathbf{A_d}(\boldsymbol{\psi}(k))\hat{\boldsymbol{x}}(k) + \mathbf{B_d}\boldsymbol{u}(k) + \mathbf{L_d}(\boldsymbol{\psi}(k))(\boldsymbol{y}(k) - \hat{\boldsymbol{y}}(k)) \tag{103}$$

$$\hat{\boldsymbol{y}}(k) = \mathbf{C}\hat{\boldsymbol{x}}(k) \tag{104}$$

where $\hat{\boldsymbol{x}}(k) \in \mathbb{R}^{n_x}$ and $\hat{\boldsymbol{y}}(k) \in \mathbb{R}^{n_y}$ are the estimated state and output, respectively. The matrix $\mathbf{L_d}(\boldsymbol{\psi}(k)) \in \mathbb{R}^{n_y \times n_x}$ is the gain of the LPV state observer.

The LPV controller matrix $\mathbf{K_d}(\boldsymbol{\psi}(k))$ and the LPV observer matrix $\mathbf{L_d}(\boldsymbol{\psi}(k))$ are designed in order to satisfy the specification of pole placement in a region of the complex plane.

5.1. State Reference and Feedforward Action

In order to implement the control law (102), the reference trajectory $\boldsymbol{r}(k)$, given by a desired yaw angle $\theta_h^r(k)$ and a desired pitch angle $\theta_v^r(k)$, is transformed into a state reference $\boldsymbol{x_r}(k)$ and a feedforward control action $\boldsymbol{u_r}(k)$ that correspond to an equilibrium point for the reference. The desired angles, along with the actual angles $\theta_h(k)$ and $\theta_v(k)$, are used to obtain a reference for the horizontal and vertical velocities $\Omega_h^r(k)$ and $\Omega_v^r(k)$. The desired horizontal and vertical velocities are considered to be the velocities needed to drive the system from the actual angles $\theta_h(k)$ and $\theta_v(k)$ to the desired ones $\theta_h^r(k)$ and $\theta_v^r(k)$ in the times τ_h and τ_v, respectively:

$$\Omega_h^r(k) = \left(\theta_h^r(k) - \theta_h(k)\right)/\tau_h \tag{105}$$

$$\Omega_v^r(k) = \left(\theta_v^r(k) - \theta_v(k)\right)/\tau_v \tag{106}$$

The state reference $\boldsymbol{x_r}(k)$ is given by $\boldsymbol{x_r}(k) = [\omega_h^r(k), \Omega_h^r(k), \theta_h^r(k), \omega_v^r(k), \Omega_v^r(k), \theta_v^r(k)]^T$ while the feedforward action $\boldsymbol{u_r}(k)$ is given by $\boldsymbol{u_r}(k) = [u_h^r(k), u_v^r(k)]$, where $\omega_h^r(k)$, $\omega_v^r(k)$, $u_h^r(k)$ and $u_v^r(k)$ can be obtained from the TRMS model (1)-(6) by imposing all derivatives equal to zero and $\Omega_h(k) = \Omega_h^r(k)$, $\Omega_v(k) = \Omega_v^r(k)$, $\theta_h(k) = \theta_h^r(k)$, $\theta_v(k) = \theta_v^r(k)$. This leads to the solution:

$$f_5^r(\theta_h^r, \theta_v^r) = \frac{g\left(K_C \sin\theta_v^r + (K_B - K_A)\cos\theta_v^r\right) + k_{ov}\Omega_v^r + (\Omega_h^r)^2 K_H \sin\theta_v^r \cos\theta_v^r}{l_m + k_g \Omega_h^r \cos\theta_v^r} \tag{107}$$

$$f_2^r(\theta_h^r, \theta_v^r) = \frac{f_3(\theta_h^r) - f_6(\theta_v^r) + k_{oh}\Omega_h^r - \frac{k_m \omega_v^r \sin\theta_v^r \Omega_v^r \left(K_D \cos^2\theta_v^r - K_E \sin^2\theta_v^r - K_F - 2K_E \cos^2\theta_v^r\right)}{K_D \cos^2\theta_v^r + K_E \sin^2\theta_v^r + K_F}}{l_t \cos\theta_v^r} \tag{108}$$

$$\omega_h^r(\theta_h^r, \theta_v^r) = \begin{cases} \sqrt{f_2^r / k_{fhp}} & if\ f_2^r \geq 0 \\ -\sqrt{-f_2^r / k_{fhn}} & if\ f_2^r < 0 \end{cases} \tag{109}$$

$$\omega_v^r(\theta_h^r, \theta_v^r) = \begin{cases} \sqrt{f_5^r / k_{fvp}} & if\ f_5^r \geq 0 \\ -\sqrt{-f_5^r / k_{fvn}} & if\ f_5^r < 0 \end{cases} \tag{110}$$

$$u_h^r(\theta_h^r, \theta_v^r) = \frac{(B_{tr} R_a + k_a^2)\omega_h^r + f_1(\omega_h^r) R_a}{k_a k_1} \tag{111}$$

$$u_v^r(\theta_h^r, \theta_v^r) = \frac{(B_{mr} R_a + k_a^2)\omega_v^r + f_4(\omega_v^r) R_a}{k_a k_2} \tag{112}$$

where $f_2^r(\theta_h^r, \theta_v^r)$ and $f_5^r(\theta_h^r, \theta_v^r)$ are the values of the non-linear functions $f_2(\omega_h)$ and $f_5(\omega_v)$ that correspond to the equilibrium for the desired horizontal and vertical angles and angular velocities.

5.2. LMI Pole Placement

An LMI approach for the state feedback design by pole placement constraints is described in (Chilali & Gahinet, 1996). The main motivation for seeking pole clustering in specific regions of the complex plane is that, by constraining the eigenvalues to lie in a predefined region, stability can be guaranteed and a satisfactory transient response can be ensured. A subset $\mathcal{D}$ of the complex plane is called an LMI region if there exist a symmetric matrix $\boldsymbol{\alpha} = [\alpha_{kl}] \in \mathbb{R}^{m\times m}$ and a matrix $\boldsymbol{\beta} = [\beta_{kl}] \in \mathbb{R}^{m\times m}$ such that:

$$\mathcal{D} = \{z \in \mathbb{C} : \mathbf{f}_{\mathcal{D}}(z) < 0\} \tag{113}$$

with:

$$\mathbf{f}_{\mathcal{D}}(z) := \boldsymbol{\alpha} + z\boldsymbol{\beta} + \bar{z}\boldsymbol{\beta}^T = \left[\alpha_{kl} + \beta_{kl}z + \beta_{lk}\bar{z}\right]_{1\leqslant k,l\leqslant m} \tag{114}$$

Using Gutman's theorem for LMI regions (Gutman & Jury, 1981), pole location in a given LMI region can be characterized in terms of the $m \times m$ block matrix:

$$\mathbf{Z}_{\mathcal{D}}(\mathbf{Y}, \mathbf{X}) := \boldsymbol{\alpha} \otimes \mathbf{X} + \boldsymbol{\beta} \otimes (\mathbf{YX}) + \boldsymbol{\beta}^T \otimes (\mathbf{YX})^T = \left[\alpha_{kl}\mathbf{X} + \beta_{kl}\mathbf{YX} + \beta_{lk}\mathbf{X}\mathbf{Y}^T\right]_{1\leqslant k,l\leqslant m} \tag{115}$$

where $\otimes$ denotes the Kronecker product. Then, a matrix $\mathbf{Y}$ is $\mathcal{D}$-stable (that is, all its eigenvalues lie in $\mathcal{D}$) if and only if there exists a symmetric positive definite matrix $\mathbf{X} > 0$ such that:

$$\mathbf{Z}_{\mathcal{D}}(\mathbf{Y}, \mathbf{X}) < 0 \tag{116}$$

$\mathbf{Z}_{\mathcal{D}}(\mathbf{Y}, \mathbf{X})$ in (115) and $\mathbf{f}_{\mathcal{D}}(z)$ in (114) are related by the substitution $(\mathbf{X}, \mathbf{YX}, \mathbf{XY}^T) \leftrightarrow (1, z, \bar{z})$.

Hereafter, the LMI regions considered for the design of the LPV controller and observer are the disk of radius r and center $(-q, 0)$ and the vertical strip defined by the extreme values S_{min} and S_{max}.

The disk of radius r and center $(-q, 0)$ is an LMI region with characteristic function:

$$\mathbf{f}_{\mathcal{D}}(z) = \begin{pmatrix} -r & q+z \\ q+\bar{z} & -r \end{pmatrix} \tag{117}$$

such that (116) leads to:

$$\begin{pmatrix} -r\mathbf{X} & q\mathbf{X} + \mathbf{Y}\mathbf{X} \\ q\mathbf{X} + \mathbf{X}\mathbf{Y}^T & -r\mathbf{X} \end{pmatrix} < 0 \tag{118}$$

The vertical strip with extreme values S_{min} and S_{max} is an LMI region with characteristic function:

$$\mathbf{f}_{\mathcal{D}}(z) = \begin{pmatrix} S_{\min} - (z + \bar{z})/2 & 0 \\ 0 & (z + \bar{z})/2 - S_{\max} \end{pmatrix} \tag{119}$$

such that (116) leads to:

$$\begin{pmatrix} S_{\min}\mathbf{X} - (\mathbf{Y}\mathbf{X} + \mathbf{X}\mathbf{Y}^T)/2 & 0 \\ 0 & (\mathbf{Y}\mathbf{X} + \mathbf{X}\mathbf{Y}^T)/2 - S_{\max}\mathbf{X} \end{pmatrix} < 0 \tag{120}$$

The LMI describing the region of the complex plane obtained through intersection of the circle and the vertical strip can be obtained easily, because the class of LMI regions is invariant under set intersection. Specifically, given two LMI regions $\mathcal{D}_1$ and $\mathcal{D}_2$ and their associated characteristic functions $\mathbf{f}_{\mathcal{D}\mathbf{1}}$ and $\mathbf{f}_{\mathcal{D}\mathbf{2}}$, the intersection $\mathcal{D} = \mathcal{D}_1 \cap \mathcal{D}_2$ is also an LMI region with characteristic function $\mathbf{f}_{\mathcal{D}} = diag(\mathbf{f}_{\mathcal{D}\mathbf{1}}, \mathbf{f}_{\mathcal{D}\mathbf{2}})$. A consequence of this intersection property is that simultaneous clustering constraints can be expressed as a system of LMIs in the same variable $\mathbf{X}$ without introducing any conservatism (Chilali & Gahinet, 1996). Given two LMI regions $\mathcal{D}_1$ and $\mathcal{D}_2$, a matrix $\mathbf{Y}$ is both $\mathcal{D}_1$-stable and $\mathcal{D}_2$-stable if and only if there exists a positive definite matrix $\mathbf{X} > 0$ such that $\mathbf{Z}_{\mathcal{D}\mathbf{1}}(\mathbf{Y}, \mathbf{X}) < 0$ and $\mathbf{Z}_{\mathcal{D}\mathbf{2}}(\mathbf{Y}, \mathbf{X}) < 0$.

5.3. Controller Design

Consider a discrete-time linear parameter-varying (LPV) system described by:

$$\begin{cases} \boldsymbol{x}(k+1) = \mathbf{A}_{\mathbf{d}}\left(\boldsymbol{\psi}_{\boldsymbol{d}}(k)\right)\boldsymbol{x}(k) + \mathbf{B}_{\mathbf{d}}\boldsymbol{u}(k) \\ \boldsymbol{y}(k) = \mathbf{C}\boldsymbol{x}(k) \end{cases} \tag{121}$$

under state-feedback control law $\boldsymbol{u}(k) = \mathbf{K}_{\mathbf{d}}\left(\boldsymbol{\psi}_{\boldsymbol{d}}(k)\right)\boldsymbol{x}(k)$. The problem to be solved consists in finding a state-feedback gain $\mathbf{K}_{\mathbf{d}}$ scheduled by $\boldsymbol{\psi}_{\boldsymbol{d}}$ that places the closed-loop poles of (121) in some LMI region $\mathcal{D}$ with characteristic function (114). Notice that, following Ghersin & Sanchez-Peña (2002) and with a little abuse of language, we define the poles of an LPV system as the set of all the poles of the LTI systems obtained by freezing $\boldsymbol{\psi}_{\boldsymbol{d}}(k)$ to some given value $\boldsymbol{\psi}_{\boldsymbol{d}}^{*}$.

Hence, the pole-placement constraint is satisfied if and only if there exists a symmetric positive definite matrix $\mathbf{X} > 0$ such that:

$$\left\{\alpha_{kl}\mathbf{X} + \beta_{kl}\left[\mathbf{A_d}\left(\boldsymbol{\psi}_d^*\right) + \mathbf{B_d}\mathbf{K_d}\left(\boldsymbol{\psi}_d^*\right)\right]\mathbf{X} + \beta_{lk}\mathbf{X}\left[\mathbf{A_d}\left(\boldsymbol{\psi}_d^*\right) + \mathbf{B_d}\mathbf{K_d}\left(\boldsymbol{\psi}_d^*\right)\right]^T\right\}_{1\leqslant k,l\leqslant m} < 0 \tag{122}$$

is satisfied for all possible values of $\boldsymbol{\psi}_d^*$.

By means of the auxiliary variable $\boldsymbol{\Gamma}_d\left(\boldsymbol{\psi}_d^*\right) := \mathbf{K_d}\left(\boldsymbol{\psi}_d^*\right)\mathbf{X}$ the matrix inequality (122) becomes an LMI, that can be solved through convex optimization techniques:

$$\left\{\alpha_{kl}\mathbf{X} + \beta_{kl}\left[\mathbf{A_d}\left(\boldsymbol{\psi}_d^*\right)\mathbf{X} + \mathbf{B_d}\boldsymbol{\Gamma}_d\left(\boldsymbol{\psi}_d^*\right)\right] + \beta_{lk}\left[\mathbf{A_d}\left(\boldsymbol{\psi}_d^*\right)\mathbf{X} + \mathbf{B_d}\boldsymbol{\Gamma}_d\left(\boldsymbol{\psi}_d^*\right)\right]^T\right\}_{1\leqslant k,l\leqslant m} < 0 \tag{123}$$

Notice that a problem associated with (123) is that this LMI formulation imposes infinite constraints. One effective way to solve this problem is reducing the LMI constraints to a finite number through polytopic LPV modeling. In this case, not only the system but also the control law (102) is expressed in a polytopic way as follows:

$$\boldsymbol{u}(k) = \boldsymbol{u_r}(k) + \sum_{i=1}^{N} \pi_i\left(\boldsymbol{\psi}(k)\right)\mathbf{K}_{\mathbf{d},i}\left(\hat{\boldsymbol{x}}(k) - \boldsymbol{x_r}(k)\right) \tag{124}$$

and the problem reduces in computing state-feedback gains $\mathbf{K}_{\mathbf{d},i}$ appearing in (124) and a single Lyapunov matrix $\mathbf{X} = \mathbf{X}^T > 0$ such that $\mathbf{Z}_{\mathcal{D}}(\mathbf{A}_{\mathbf{d},i}+\mathbf{B_d}\mathbf{K}_{\mathbf{d},i}, \mathbf{X}) < 0$ for $i = 1, \ldots, N$. The use of a single Lyapunov function over the entire operating range guarantees $\mathcal{D}-$stability for all state-space matrices in the polytope (65).

Summarizing, let $\mathcal{D}$ be an LMI region, and suppose that the LPV system is quadratically $\mathcal{D}$-stabilizable with a symmetric positive definite Lyapunov matrix $\mathbf{X}$ and state-feedback gains $\mathbf{K}_{\mathbf{d},i}$, and let $\boldsymbol{\Gamma}_i = \mathbf{K}_{\mathbf{d},i}\mathbf{X}$. Writing the condition $\mathbf{Z}_{\mathcal{D}}(\mathbf{A}_{\mathbf{d},i} + \mathbf{B_d}\mathbf{K}_{\mathbf{d},i}, \mathbf{X}) < 0$ at each vertex $(\mathbf{A}_{\mathbf{d},i}, \mathbf{B_d})$ of the polytope (65) yields the following necessary conditions on $\mathbf{X}$ and $\boldsymbol{\Gamma}_i$:

$$\begin{cases} \left[\alpha_{kl}\mathbf{X} + \beta_{kl}(\mathbf{A}_{\mathbf{d},i}\mathbf{X} + \mathbf{B_d}\boldsymbol{\Gamma}_i) + \beta_{lk}(\mathbf{A}_{\mathbf{d},i}\mathbf{X} + \mathbf{B_d}\boldsymbol{\Gamma}_i)^T\right]_{k,l} < 0 \\ \mathbf{X} > 0 \end{cases} \tag{125}$$

for $i = 1, \ldots, N$. Conditions (125) are necessary and sufficient for quadratic $\mathcal{D}$-stabilizability.

Thus, pole-placement in the intersection between the disk of radius r_K and center $(-q_K, 0)$ and the vertical strip with extreme values S_{minK} and S_{maxK} is obtained

solving the following system of LMIs:

$$\begin{cases} diag(\mathbf{Q}_1, \mathbf{Q}_2, \ldots, \mathbf{Q}_i, \ldots, \mathbf{Q}_N) < 0 \\ \mathbf{X} > 0 \end{cases} \tag{126}$$

with each $\mathbf{Q}_i$ defined at the i^{th} vertex of the polytopic system as follows:

$$\begin{cases} \mathbf{Q}_i = diag\left(\mathbf{Q}_i^1, \mathbf{Q}_i^2, \mathbf{Q}_i^3\right) \\ \mathbf{Q}_i^1 = \begin{pmatrix} -r_K\mathbf{X} & q_K\mathbf{X} + \mathbf{A}_{\mathbf{d},i}\mathbf{X} + \mathbf{B}_\mathbf{d}\mathbf{\Gamma}_i \\ q_K\mathbf{X} + \mathbf{X}\mathbf{A}_{\mathbf{d},i}^T + \mathbf{\Gamma}_i^T\mathbf{B}_\mathbf{d}{}^T & -r_K\mathbf{X} \end{pmatrix} \\ \mathbf{Q}_i^2 = S_{\min K}\mathbf{X} - \frac{1}{2}\left(\mathbf{A}_{\mathbf{d},i}\mathbf{X} + \mathbf{X}\mathbf{A}_{\mathbf{d},i}^T + \mathbf{B}_\mathbf{d}\mathbf{\Gamma}_i + \mathbf{\Gamma}_i^T\mathbf{B}_\mathbf{d}{}^T\right) \\ \mathbf{Q}_i^3 = \frac{1}{2}\left(\mathbf{A}_{\mathbf{d},i}\mathbf{X} + \mathbf{X}\mathbf{A}_{\mathbf{d},i}^T + \mathbf{B}_\mathbf{d}\mathbf{\Gamma}_i + \mathbf{\Gamma}_i^T\mathbf{B}_\mathbf{d}{}^T\right) - S_{\max K}\mathbf{X} \end{cases} \tag{127}$$

Once this system of LMIs is solved, the controller gains $\mathbf{K}_{\mathbf{d},i}$ can be determined by $\mathbf{K}_{\mathbf{d},i} = \mathbf{\Gamma}_i\mathbf{X}^{-1}$.

5.4. Integral Action

Integral control is needed in order to eliminate the steady-state errors due to some imperfections in either the modeling or the identification of the TRMS. For this reason, some form of integral control is typically included in most control systems that do not contain natural integrators. The control that has been used so far is an extension of state-space design methods to LPV systems: state-space designs will not naturally include an integral action unless additional steps are taken. A method to add an integral action to classic state-space control is described in (Franklin et al., 1997) and it is based on state augmentation: the state is augmented in such a way that the control system achieves zero steady-state error for a general class of reference and disturbance signals.

The idea is to add a state to obtain an integral of the error signal. This integrator is implemented as part of the controller equations. Then, the integral is fed-back along with the estimated or measured state. To accomplish the design of the feedback gains for both the integral and the original state vector, the model of the plant is augmented and an integral error output is added to the existing plant state output. This augmented model is then used as before to calculate the feedback control gains for the augmented model.

More specifically, the state of the system (121) is augmented with $\boldsymbol{x}_I$, the integral of the error $\boldsymbol{e} = \boldsymbol{y} - \boldsymbol{r}$. The discrete-time integral results in a summation of all past values of $\boldsymbol{e}(k)$, that is:

$$\boldsymbol{x}_I(k+1) = \boldsymbol{x}_I(k) + \boldsymbol{e}(k) = \boldsymbol{x}_I(k) + \mathbf{C}\boldsymbol{x}(k) - \boldsymbol{r}(k) \tag{128}$$

therefore arriving to the augmented plant model:

$$\begin{bmatrix} \boldsymbol{x}(k+1) \\ \boldsymbol{x}_I(k+1) \end{bmatrix} = \begin{pmatrix} \mathbf{A_d}\left(\boldsymbol{\psi}_d(k)\right) & \mathbf{0} \\ \mathbf{C} & \mathbf{I} \end{pmatrix} \begin{bmatrix} \boldsymbol{x}(k) \\ \boldsymbol{x}_I(k) \end{bmatrix} + \begin{pmatrix} \mathbf{B_d} \\ \mathbf{0} \end{pmatrix} \boldsymbol{u}(k) - \begin{pmatrix} \mathbf{0} \\ \mathbf{I} \end{pmatrix} \boldsymbol{r}(k) \tag{129}$$

With this new definition of the system, the design technique explained in Section 5.3 can be directly applied for the control law design. Notice, however, that the addition of extra poles for the integrator state element will typically lead to a deteriorated performance of the response in comparison with the one obtained without integral control.

5.5. Observer Design

Consider a discrete-time LPV system and the LPV state observer described by:

$$\begin{cases} \boldsymbol{x}(k+1) = \mathbf{A_d}\left(\boldsymbol{\psi}_d(k)\right)\boldsymbol{x}(k) + \mathbf{B_d}\boldsymbol{u}(k) \\ \boldsymbol{y}(k) = \mathbf{C}\boldsymbol{x}(k) \\ \hat{\boldsymbol{x}}(k+1) = \mathbf{A_d}\left(\boldsymbol{\psi}_d(k)\right)\hat{\boldsymbol{x}}(\boldsymbol{k}) + \mathbf{B_d}\boldsymbol{u}(k) + \mathbf{L_d}\left(\boldsymbol{\psi}_d(k)\right)\left(\hat{\boldsymbol{y}}(k) - \boldsymbol{y}(k)\right) \\ \hat{\boldsymbol{y}}(k) = \mathbf{C}\hat{\boldsymbol{x}}(k) \end{cases} \tag{130}$$

The problem to be solved consists in finding a gain $\mathbf{L_d}$, scheduled by $\boldsymbol{\psi}_d$, that places the closed-loop poles of the observer (130) in an LMI region $\mathcal{D}$ with characteristic function (114). Here, as in the state-feedback controller case and following Ghersin & Sanchez-Peña (2002), we define the poles of the LPV observer as the set of all the poles of the LTI observers obtained by freezing $\boldsymbol{\psi}_d(k)$ to some given value $\boldsymbol{\psi}_d^*$.

Thanks to the duality property, this is equivalent to the problem of finding a state-feedback gain ${\mathbf{L_d}}^T$, scheduled by $\boldsymbol{\psi}_d$, that places the poles of the closed-loop dual system in $\mathcal{D}$:

$$\begin{cases} \boldsymbol{z}(k+1) = {\mathbf{A_d}}^T\left(\boldsymbol{\psi}_d(k)\right)\boldsymbol{z}(k) + \mathbf{C}^T\boldsymbol{v}(k) \\ \boldsymbol{w}(k) = {\mathbf{B_d}}^T\boldsymbol{z}(k) \end{cases} \tag{131}$$

under the state-feedback control law $\boldsymbol{v}(k) = {\mathbf{L_d}}^T\left(\boldsymbol{\psi}_d(k)\right)\boldsymbol{z}(k)$. In other words, $\mathcal{D}$-detectability of the pair $\left(\mathbf{A_d}\left(\boldsymbol{\psi}_d(k)\right), \mathbf{C}\right)$ is equivalent to $\mathcal{D}$-stabilizability of $({\mathbf{A_d}}^T\left(\boldsymbol{\psi}_d(k)\right), \mathbf{C}^T)$ and what has already been described in Section 5.2 can be used for the design of the LPV observer (Apkarian et al., 1995).

The LPV observer is expressed in a polytopic way as follows:

$$\hat{\boldsymbol{x}}(k+1) = \sum_{i=1}^{N} \pi_i\left(\boldsymbol{\psi}_d(k)\right)\left[\mathbf{A_{d},}_i\hat{\boldsymbol{x}}(\boldsymbol{k}) + \mathbf{L_{d},}_i\left(\mathbf{C}\hat{\boldsymbol{x}}(k) - \boldsymbol{y}(k)\right)\right] + \mathbf{B_d}\boldsymbol{u}(k) \tag{132}$$

Then, the pole-placement in the intersection between the disk of radius r_L and center $(-q_L, 0)$ and the vertical strip with extreme values S_{minL} and S_{maxL} is obtained solving the following system of LMIs:

$$\begin{cases} diag(\mathbf{R}_1, \mathbf{R}_2, \ldots, \mathbf{R}_i, \ldots, \mathbf{R}_N) < 0 \\ \mathbf{X} > 0 \end{cases} \tag{133}$$

with each $\mathbf{R}_i$ defined at the i^{th} vertex of the polytopic system as follows:

$$\begin{cases} \mathbf{R}_i = diag\left(\mathbf{R}_i^1, \mathbf{R}_i^2, \mathbf{R}_i^3\right) \\ \mathbf{R}_i^1 = \begin{pmatrix} -r_L\mathbf{X} & q_L\mathbf{X} + \mathbf{A}_{\mathbf{d},i}^T\mathbf{X} + \mathbf{C}^T\mathbf{\Gamma}_i \\ q_L\mathbf{X} + \mathbf{X}\mathbf{A}_{\mathbf{d},i} + \mathbf{\Gamma}_i^T\mathbf{C} & -r_L\mathbf{X} \end{pmatrix} \\ \mathbf{R}_i^2 = S_{\min L}\mathbf{X} - \frac{1}{2}\left(\mathbf{A}_{\mathbf{d},i}^T\mathbf{X} + \mathbf{X}\mathbf{A}_{\mathbf{d},i} + \mathbf{C}^T\mathbf{\Gamma}_i + \mathbf{\Gamma}_i^T\mathbf{C}\right) \\ \mathbf{R}_i^3 = \frac{1}{2}\left(\mathbf{A}_{\mathbf{d},i}^T\mathbf{X} + \mathbf{X}\mathbf{A}_{\mathbf{d},i} + \mathbf{C}^T\mathbf{\Gamma}_i + \mathbf{\Gamma}_i^T\mathbf{C}\right) - S_{\max L}\mathbf{X} \end{cases} \tag{134}$$

Once this LMIs system is solved, the controller gains $\mathbf{L}_{\mathbf{d},i}$ can be determined by $\mathbf{L}_{\mathbf{d},i} = (\mathbf{\Gamma}_i\mathbf{X}^{-1})^T$.

5.6. Further considerations

It appears clearly that the design parameters in both the controller and the observer cases, are the LMI regions, denoted hereafter as $\mathcal{D}_K$ and $\mathcal{D}_L$, and described by the characteristic functions $\mathbf{f}_{\mathcal{D}_K}(z)$ and $\mathbf{f}_{\mathcal{D}_L}(z)$, respectively.

The choice of the two regions depends on many factors. First of all, it is known from the LTI system theory that the position of the poles of a system affects its dynamics, with each pole affecting one of the system modes. As reported by Ghersin & Sanchez-Peña (2002), it has been noticed that a similar relationship between pole placement in the LPV sense and the dynamics of an LPV system holds. Hence, a first criterion to choose $\mathcal{D}_K$ and $\mathcal{D}_L$ is based on the desired dynamics of the closed-loop system and the state observer, with the observer chosen to be faster than the controlled system. However, as it happens in the LTI case, the presence of saturations in the actuators and high-frequency noise in the sensors limits the dynamics of the closed-loop system and the observer, respectively, thus putting a limitation on the possible regions $\mathcal{D}_K$ and $\mathcal{D}_L$ that can be chosen for the design [2]. It must also be taken into account that for a given choice of $\mathcal{D}_K$

[2] A synthesis approach to design controllers with guaranteed stability and performance despite the presence of saturations is provided by Wu et al. (2000), where saturation indicator parameters are used to schedule accordingly the LPV controller. In this paper, the saturations have not been

($\mathcal{D}_L$), the system could be not $\mathcal{D}_K$-stabilizable ($\mathcal{D}_L$-detectable). When this happens, the designer of the controller (observer) should either try with a new LMI region, or with a new polytopic model. In the first case, the new region should be chosen in such a way that hopefully the system is $\mathcal{D}_K$-stabilizable ($\mathcal{D}_L$-detectable) using it (e.g. the new region is chosen bigger, in such a way that it includes the former one). In the second case, the desired LMI region specification could be satisfiable if a different polytopic model is used (e.g. a polytopic model obtained using *Bounding diamonds* or *Convex hulls* methodologies instead of the *Bounding box* approach used in this paper, or a new *Bounding box* obtained by reducing the allowed range of variation of the elements in the scheduling vector $\boldsymbol{p}$[3]).

Finally, notice that another possible control strategy for the TRMS is to split it into the subsystems that have been utilized for identification purposes. This allows controlling each subsystem independently, so that different control loops are designed for the tail rotor, the main rotor and the aeromechanical part, whose non-linear differential equations can be rewritten in a state-space form by considering the angular speeds of the two rotors as inputs of the system. In a preliminary study of the LPV control possibilities of the TRMS, this approach was tried leading to results that were worse than the ones that have been shown in this paper. Probably, the main reason of such a worsening is that the varying parameters of the aeromechanical part depend on the rotor velocities ω_h and ω_v, giving rise to couplings that do not affect the system during the identification, that is performed in open-loop, but cannot be neglected when the system has to be controlled.

6. Results

6.1. Identification

The identification procedure has been applied to sets of data that are obtained as the response of the system to a step input voltage signal with an overlapped pseudo-random sequence. The motivation of using the pseudo-random sequence

taken into account in the design step because the technique provided by Wu et al. (2000) increases the order of the system to be controlled, thus increasing the order of the LMIs and, as a consequence, the computational burden. Therefore, it has been preferred to design the controller without taking into account the saturations and, afterwards, to check through simulations and experiments that the obtained controller did not cause the actuators to reach their limits.

[3]However, a risk associated with reducing the allowed range of variation of the elements in $\boldsymbol{p}$ is that the desired specifications would be valid only as long as the system varying parameters do not exit from the new box.

Table 6: Identified parameters values

Par.	Value	Par.	Value	Par.	Value	Par.	Value
B_{tr}	0.0086	B_{mr}	0.0026	k_{thp}	0.0027	k_{thn}	0.0028
J_{tr}	0.0059	J_{mr}	0.0254	k_t	0	k_m	0.0017
k_{tvp}	0.0168	k_{tvn}	0.0155	k_{oh}	0.0185	k_{ov}	0.1026
k_{fhp}	0.0566	k_{fhn}	0.0660	k_{fvp}	0.3819	k_{fvn}	0.2197
k_{chp}	0.0158	k_{chn}	0.0111	k_{cvp}	0.0623	k_{cvn}	0.0563

is due to its properties that are similar to those of the white noise, allowing a persistent excitation of the system to be identified.

The minima of (70), (71), (89), (95) and (101) are found by means of *fmincon* MATLAB function of the Optimization Toolbox (Coleman et al., 2011). This function attempts to find a constrained minimum of a scalar function of several variables (in this case, the unknown parameters). This is generally referred to as constrained non-linear optimization or non-linear programming. The values returned by the *fmincon* functions are listed in Table 6.

Fig. 2, Fig. 3, Fig. 4, Fig. 5 and Fig. 6 show the comparison between the validation data obtained from the real set-up and the predicted data obtained from the identified model. Each figure is divided into three subfigures. In the first one, the TRMS time response is plotted against the nonlinear model one. In the second subfigure, the prediction error is shown. Finally, in the third subfigure, the power spectral density (PSD) of the model is compared with the PSD of the real data. It can be seen that the model prediction fits well the real data in both the time and frequency domains. The difference between the model and the TRMS in the high-frequency PSD is small enough so as to let think that using other excitation signals for improving the goodness of the model is not necessary.

Notice that the absence of the non-linear Coulomb friction and stiction in the model can be seen when the angular velocity of either the main or the tail propeller is near to zero (see Fig. 7, where the response of the tail rotor excited by an input signal generated with values obtained each second from a Gaussian distribution with mean $u_h^{mean} = 0.05\,V$ and standard deviation $\sigma_{u_h} = 0.05\,V$ is shown). However, since the working points of the propellers are usually different than $0\,rad/s$, and the controller has an inherent robustness against small model imperfections, these effects have been neglected. Considering the two above mentioned effects would improve the goodness of the model, even though it would complicate the identification procedure.

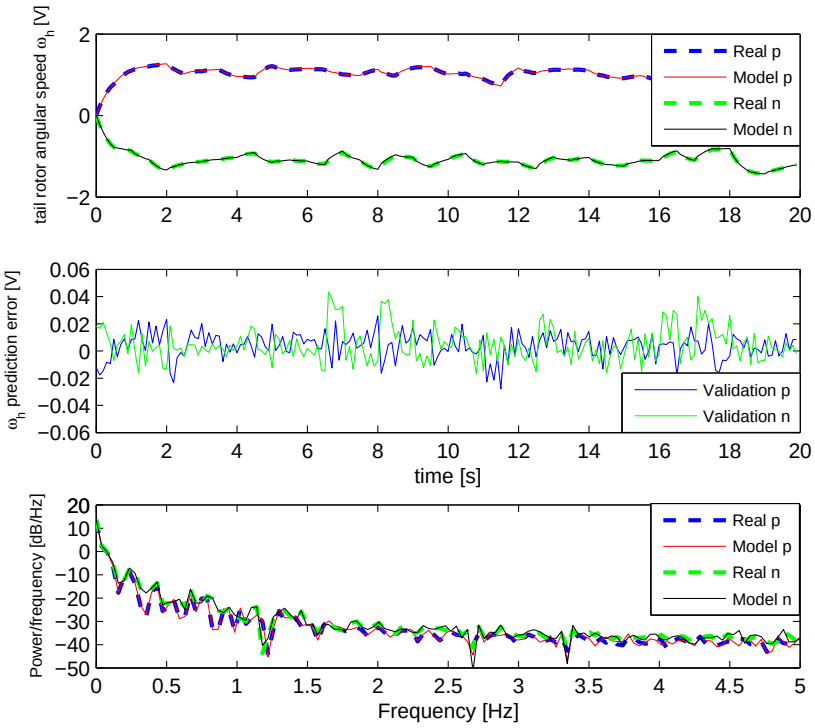

Figure 2: Tail rotor parameters identification. p: Validation experiment with positive input values. n: Validation experiment with negative input values.

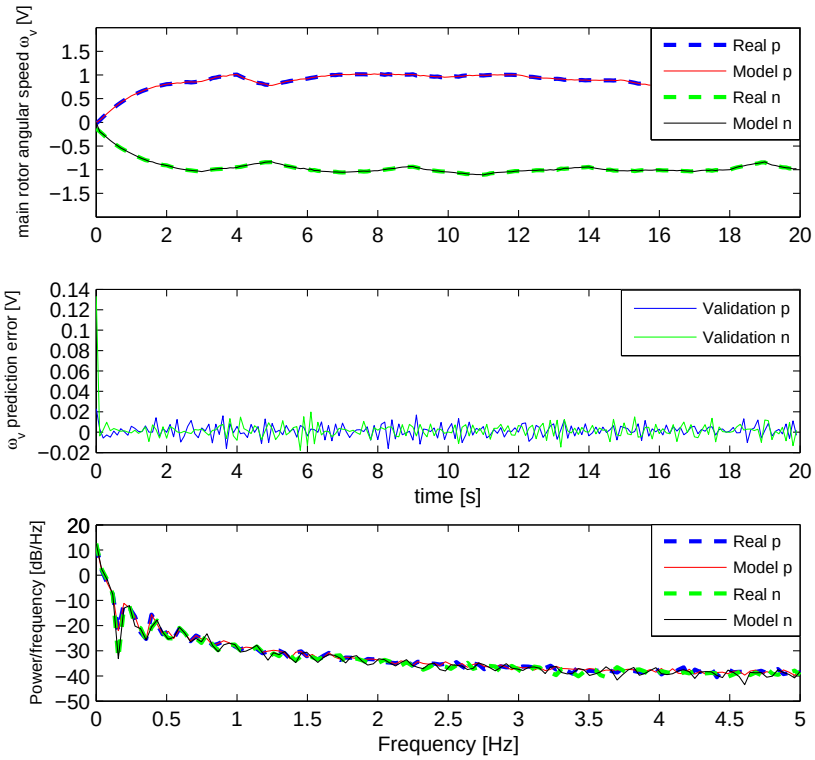

Figure 3: Main rotor parameters identification. p: Validation experiment with positive input values. n: Validation experiment with negative input values.

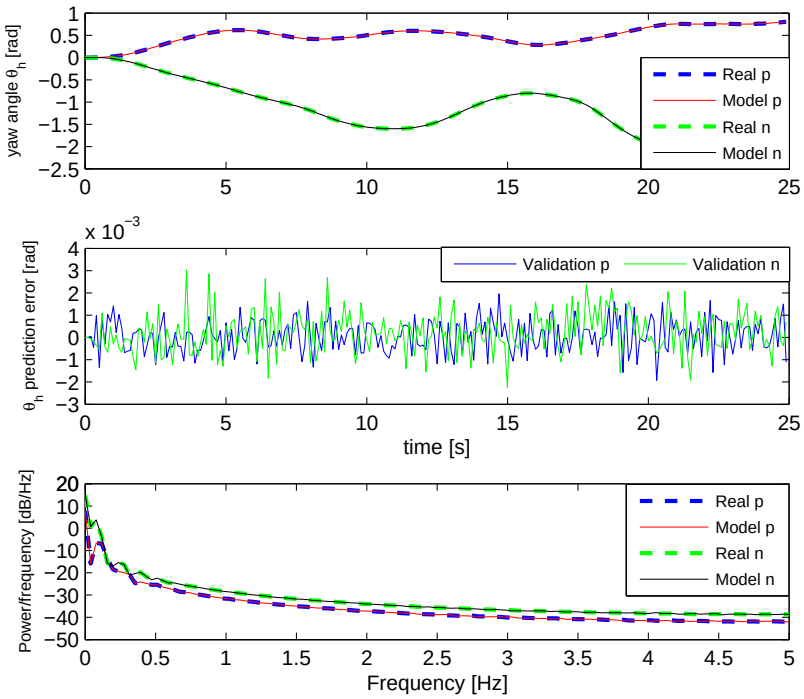

Figure 4: Tail propeller to horizontal aeromechanical parameters identification. p: Validation experiment with positive input values. n: Validation experiment with negative input values.

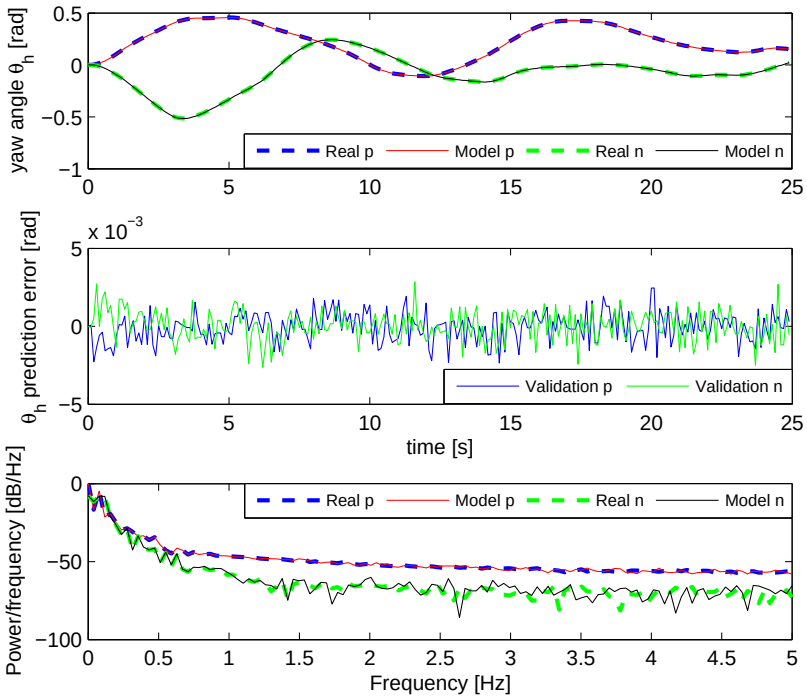

Figure 5: Main propeller to horizontal aeromechanical parameters identification. p: Validation experiment with positive input values. n: Validation experiment with negative input values.

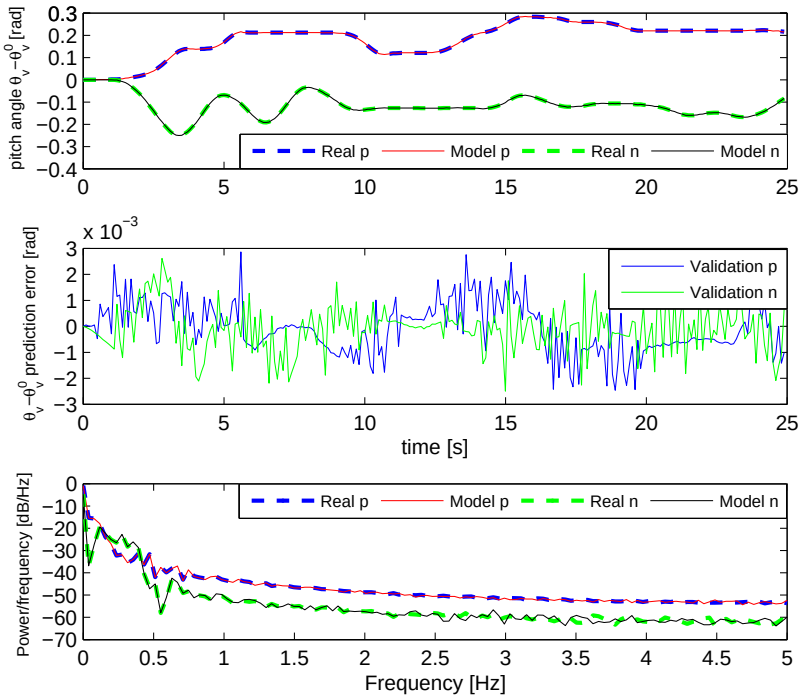

Figure 6: Main propeller to vertical aeromechanical parameters identification. p: Validation experiment with positive input values. n: Validation experiment with negative input values.

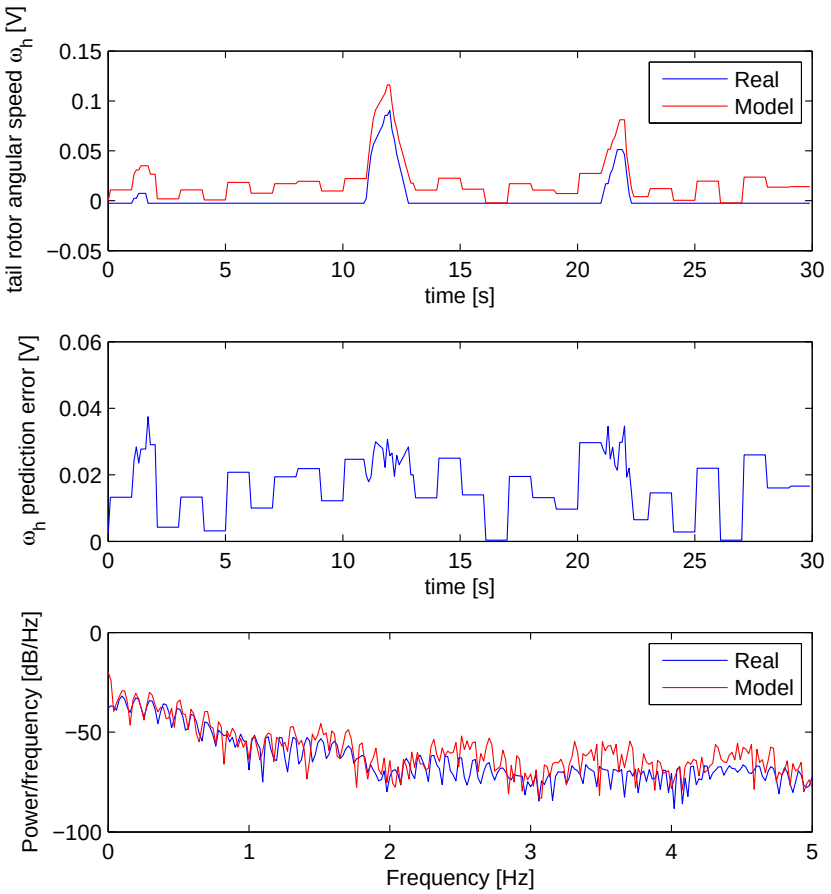

Figure 7: Tail rotor propeller response with an input signal of mean $u_h^{mean} = 0.05V$.

Table 7: State variables limits

Variable	Minimum	Maximum	Variable	Minimum	Maximum
u_h	-2.5 V	2.5 V	u_v	-2 V	2 V
ω_h	-2.9 V	2.9 V	ω_v	-1.6 V	1.6 V
Ω_h	-1 rad/s	1 rad/s	Ω_v	-0.6 rad/s	0.6 rad/s
θ_h	-1.7 rad	1.2 rad	$\theta_v - \theta_v^0$	-0.5 rad	1.0 rad

6.2. Polytopic Bounding Box

Once the parameters of the non-linear model have been identified, a polytopic quasi-LPV model can be obtained by applying the procedure described in Section 3.5. The motor inputs u_h and u_v and each of the state variables that influence the values of the elements of the state matrix (42) is assumed to take values in an interval, as resumed in Table 7[4].

In order to design a digital controller, a discrete-time polytopic model is required. This has been obtained by using Euler approximation with sampling time $T_s = 0.1s$. Minimum and maximum values for each of the elements of the scheduling vector $\boldsymbol{\psi_d}$ have been calculated, and such values are listed in Table 8.

Remark: The choice of a sampling time $T_s = 0.1s$ is motivated by a research in the literature. In fact, the same choice has been made in Dutka et al. (2003), and a sampling time $T_s = 0.2s$ has been used in Rahideh & Shaheed (2009), for controlling the TRMS using robust model predictive control based on polytopes. Moreover, in Toha & Tokhi (2009), it is stated that *the sampling time must not be too short because poles will group around* $z = 1$. Some experiments have been performed changing the sampling time to a smaller value ($T_s = 0.01s$), leading to results similar to the ones shown in this paper.

6.3. Control

The LPV state observer is designed with LMIs (125) assuming that the eigenvalues are placed in an LMI region that is the intersection between the disk of radius $r_L = 0.7$ and center $(-q_L, 0) = (0, 0)$ and a vertical strip defined by the extreme values $S_{minL} = 0$ and $S_{maxL} = 0.7$. The application of the LPV theory would need to solve $2^N + 1$ LMIs, where N is the number of elements of the parameter

[4]Notice that the rotational velocities of the rotors ω_h and ω_v are expressed in voltage because the model has been calibrated using directly the data coming from the measurements.

Table 8: Scheduling parameters limits

ψ_{jd}	$\underline{\psi}_{jd}$	$\overline{\psi}_{jd}$	ψ_{jd}	$\underline{\psi}_{jd}$	$\overline{\psi}_{jd}$
ψ_{1d}	0.7207	0.8534	ψ_{2d}	0.0026	0.1124
ψ_{3d}	0.9122	0.9697	ψ_{4d}	-0.0750	-0.0182
ψ_{5d}	-0.0041	-0.0003	ψ_{6d}	-0.0019	0.0019
ψ_{7d}	-0.1336	0.1148	ψ_{8d}	0.8837	0.9896
ψ_{9d}	-0.0460	0.2082	ψ_{10d}	0	0.2339
ψ_{11d}	-0.4109	-0.3464			

vector $\boldsymbol{\psi_d}$. In the case of the TRMS, $N = 11$, that means 2049 LMIs have to be solved, leading to computational issues as the time needed to solve this number of LMIs increases in an exponential way with N. Hence, the design of the LPV observer is made by considering that only the $\tilde{N}$ most varying parameters change, and all the others are approximated with a constant value.

Such parameters have been found by approximating each parameter with a constant value found through least-squares algorithm (see, for example, Fig. 8 and Fig. 9 that show the approximation of some of the varying parameters). Later, the magnitude of the differences between the original non-linear model and the model obtained approximating the non-linearity embedded in the parameter taken into consideration with the corresponding linearity has been analyzed in a simulation environment.

The choice $\tilde{N} = 8$ has been found as a good compromise between computation time and performance, resulting in the reduced varying parameter vector $\boldsymbol{\psi} = [a_{11}, a_{21}, a_{22}, a_{23}, a_{26}, a_{44}, a_{54}, a_{56}]^T$.

The system of LMIs (133) has been solved using the YALMIP toolbox (Löfberg, 2004) and the SeDuMi solver (Sturm, 1999), that have returned the following Lyapunov matrix[5]:

$$\mathbf{X_L} = 10^{-3} \times \begin{pmatrix} 1.637 & 0 & 0 & 0 & 0 & 0 \\ 0 & 0.066 & -0.206 & 0 & -0.031 & 0.032 \\ 0 & -0.206 & 1.094 & 0 & 0.011 & 0.043 \\ 0 & 0 & 0 & 1.049 & 0 & 0 \\ 0 & -0.031 & 0.011 & 0 & 0.165 & -0.316 \\ 0 & 0.032 & 0.043 & 0 & -0.316 & 1.109 \end{pmatrix} \tag{135}$$

[5]Since $\tilde{N} = 8$, it is not possible to provide the 256 vertex observer gains $L_1, \ldots, L_{256}$ returned.

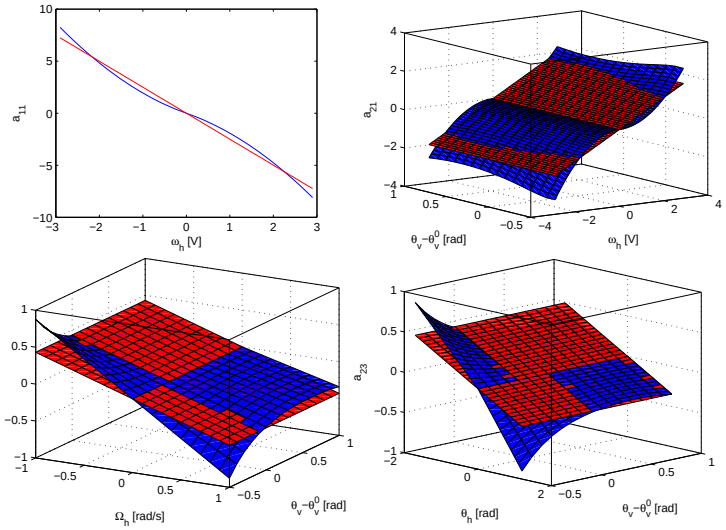

Figure 8: Parameter approximation I: a_{11}, a_{21}, a_{22} and a_{23}.

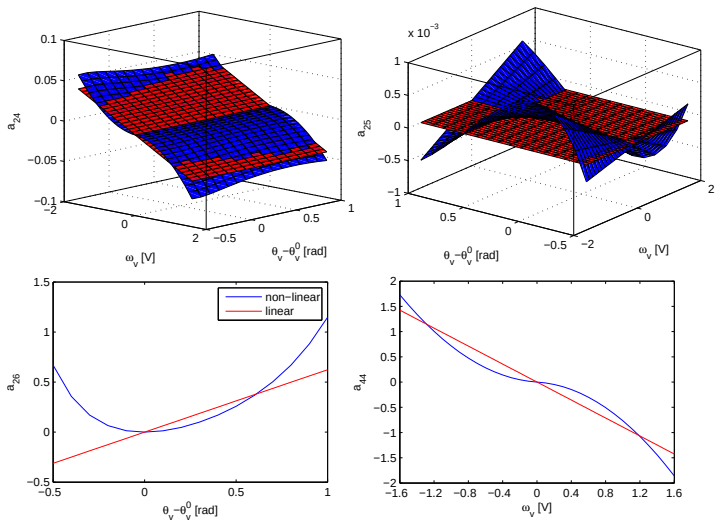

Figure 9: Parameter approximation II: a_{24}, a_{25}, a_{26} and a_{44}.

In the same way, the LPV controller is designed with LMIs (125), applied to the augmented system (129), assuming that the eigenvalues are placed in an LMI region that is the intersection between the center of radius $r_k = 0.29$ and center $(-q_k, 0) = (0.7, 0)$ and a vertical strip defined by the extreme values $S_{minK} = 0.41$ and $S_{maxK} = 0.99$. Analogously to the LPV state observer case, the design of the LPV controller is made with a number of varying parameters $\tilde{N} = 8$, and the YALMIP toolbox and SeDuMi solver have returned the following Lyapunov matrix:

$$\mathbf{X_K} = 10^{-11} \times \begin{pmatrix} 2.18 & -0.46 & 0.11 & 0.06 & 0.06 & -0.01 & -0.09 & 0 \\ -0.46 & 0.18 & -0.06 & -0.01 & -0.04 & 0.01 & -0.10 & -0.01 \\ 0.11 & -0.06 & 0.23 & 0.01 & 0.01 & 0 & -0.20 & 0.01 \\ 0.06 & -0.01 & 0.01 & 0.78 & -0.31 & 0.05 & 0.02 & -0.02 \\ 0.06 & -0.04 & 0.01 & -0.31 & 0.35 & -0.04 & 0.02 & -0.01 \\ -0.01 & 0.01 & 0 & 0.05 & -0.04 & 0.04 & 0 & -0.01 \\ -0.09 & -0.10 & -0.20 & 0.02 & 0.02 & 0 & 1.45 & -0.03 \\ 0 & -0.01 & 0.01 & -0.02 & -0.01 & -0.01 & -0.03 & 0.34 \end{pmatrix} \tag{136}$$

The experiments have been done using the following reference angle trajectories:

$$\theta_h^{ref} = \begin{cases} 0.5\frac{t}{4} & 0s \leq t < 4s \\ 0.5 & 4s \leq t < 75s \\ 0.5 + 0.2\frac{t-75}{3} & 75s \leq t < 78s \\ 0.7 & 78s \leq t < 180s \\ 0.7 - 1.3\frac{t-180}{4} & 180s \leq t < 184s \\ -0.6 & 184s \leq t \leq 300s \end{cases} \tag{137}$$

$$\theta_v^{ref} - \theta_v^0 = \begin{cases} 0.2\frac{t}{3} & 0s \leq t < 3s \\ 0.2 & 3s \leq t < 75s \\ 0.2 + 0.1\frac{t-75}{3} & 75s \leq t < 78s \\ 0.3 & 78s \leq t < 150s \\ 0.3 - 0.5\frac{t-150}{4} & 150s \leq t < 154s \\ -0.2 & 154s \leq t \leq 300s \end{cases} \tag{138}$$

To prove the convergence of the observer, the following initial conditions on the TRMS state and the observer state have been considered:

$$\begin{aligned} \mathbf{x}(0) &= \begin{bmatrix} \omega_h(0) & \Omega_h(0) & \theta_h(0) & \omega_v(0) & \Omega_v(0) & \theta_v(0) - \theta_v^0 \end{bmatrix}^T = \\ &= \begin{bmatrix} 0 & 0 & 0 & 0 & 0 & 0 \end{bmatrix}^T \end{aligned} \tag{139}$$

$$\begin{aligned}\hat{\mathbf{x}}(0) &= \begin{bmatrix} \hat{\omega}_h(0) & \hat{\Omega}_h(0) & \hat{\theta}_h(0) & \hat{\omega}_v(0) & \hat{\Omega}_v(0) & \hat{\theta}_v(0) - \theta_v^0 \end{bmatrix}^T = \\ &= \begin{bmatrix} 1 & 1 & 1 & 1 & 0.1 & 0.1 \end{bmatrix}^T \end{aligned} \tag{140}$$

Fig. 10 and Fig. 11 show a comparison between the TRMS state and the observer state. The first figure refers to simulation data, where all the TRMS state is available for comparison with the observer one. The second figure refers to real data, where the measurements of the angular velocities Ω_h and Ω_v are not available. Hence, only the other 4 states are shown and compared. In all cases, it can be seen that despite the difference in the initial conditions, the observer eventually converges.

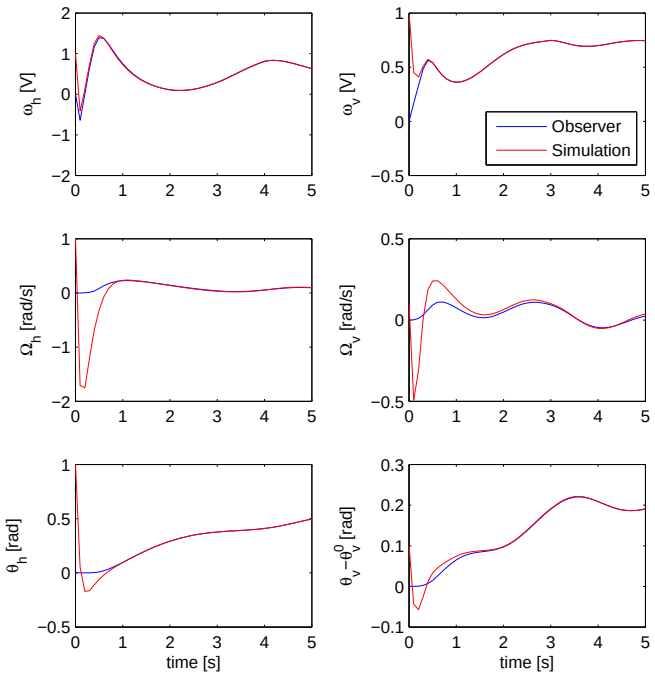

Figure 10: Observer results (simulation).

Fig. 12 and Fig. 13 show the yaw angle and the pitch angle response, respectively. Both simulation and real results are shown in the same figure. It can be seen that the TRMS follows the desired reference in both cases.

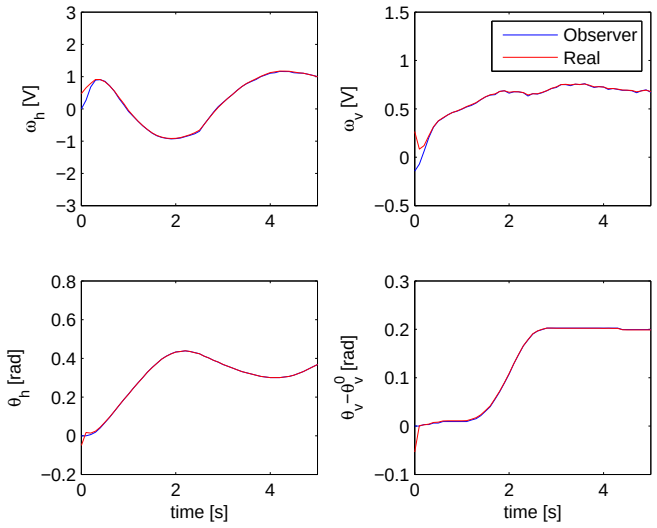

Figure 11: Observer results (real).

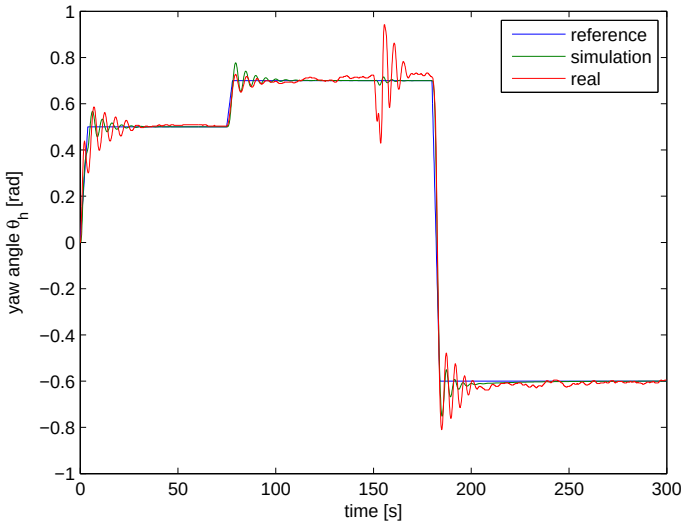

Figure 12: Control of the yaw angle θ_h.

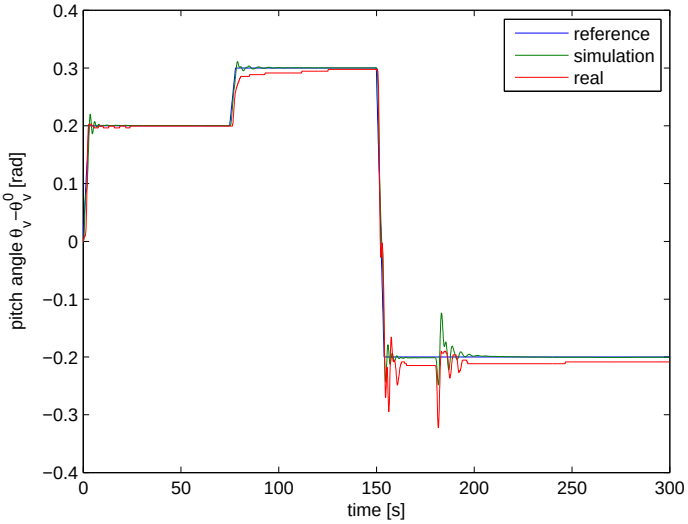

Figure 13: Control of the pitch angle $\theta_v - \theta_v^0$.

Fig. 14 shows the control signals. In the upper side of the figure, simulation control signals are shown, while in the lower side control signals in the experiment with the real set-up are shown.

7. Conclusions

This paper has proposed a quasi-LPV modeling, identification and control approach for the TRMS developed by Feedback Instruments Limited. The non-linear model of the TRMS has been transformed into a quasi-LPV system and then approximated in a polytopic way. Then, the unknown parameters of the TRMS have been identified by means of non-linear least-squares identification using data collected from the real laboratory set-up. The model showed good performance when tested against validation data. Later, using the LPV pole placement approach based on LMI regions, an LPV observer and an LPV state-feedback controller have been designed. The effectiveness and performance of the proposed approach have been proved both in a simulation environment and with the real laboratory set-up.

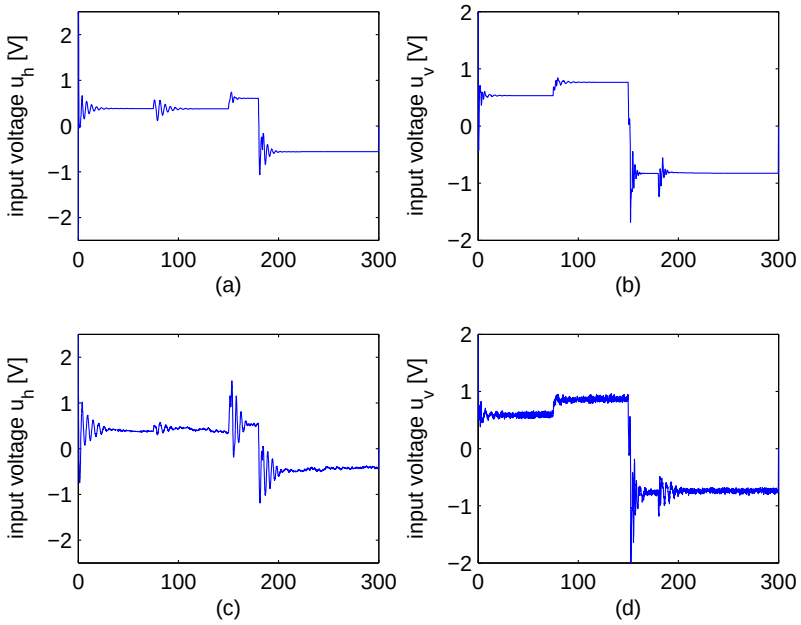

Figure 14: Control signals: (a) tail motor input voltage (simulation); (b) main motor input voltage (simulation); (c) tail motor input voltage (real); (d) main motor input voltage (real).

Acknowledgments

This work has been funded by the Spanish MINECO through the project CYCYT SHERECS (ref. DPI2011-26243), by the European Commission through contract i-Sense (ref. FP7-ICT-2009-6-270428) and by UPC through the grant FPI-UPC E-01104.

The authors would like to thank the anonymous referees for their valuable comments and suggestions, which helped to improve the paper. The authors would also like to thank Diego García Valverde for his help in the implementation of the developed algorithms to the real TRMS set-up.

References

Ahmad, S. M., Chipperfield, A. J., & Tokhi, M. O. (2002). Dynamic modelling and open-loop control of a twin rotor multi-input multi-output system. In *Proceedings of the Institution of Mechanical Engineers, Part I: Journal of Systems and Control Engineering* (pp. 477–496).

Ahmad, S. M., Shaheed, M. H., Chipperfield, A. J., & Tokhi, M. O. (2000). Nonlinear modelling of a twin rotor MIMO system using radial basis function networks. In *Proceedings of the IEEE 2000 National Aerospace and Electronics Conference* (pp. 313–320).

Ahmed, Q., Bhatti, A. I., & Iqbal, S. (2009). Nonlinear robust decoupling control design for twin rotor system. In *Proceedings of the 7th Asian Control Conference, Hong Kong, China* (pp. 937–942).

Alam, M. S., & Tokhi, M. O. (2007). Modelling of a twin rotor system: a particle swarm optimization approach. *Proceedings of the Institution of Mechanical Engineers, Part G: Journal of Aerospace Engineering*, *221*, 353–374.

Aldebrez, F. M., Darus, I. Z. M., & Tokhi, M. O. (2004). Dynamic modelling of a twin rotor system in hovering position. In *First International Symposium on Control, Communication and Signal Processing* (pp. 823–826).

Andrés, M., & Balas, G. J. (2004). Development of linear parameter varying models for aircraft. *Journal of Guidance, Control and Dynamics*, *27*, 218–228.

Apkarian, P., Gahinet, P., & Becker, G. (1995). Self-scheduled H_∞ control of linear parameter-varying systems: a design example. *Automatica*, *31*, 1251 – 1261.

Bergsten, P., Palm, R., & Driankov, D. (2002). Observers for Takagi-Sugeno Fuzzy Systems. *IEEE Transactions on Systems, Man, and Cybernetics - Part B: Cybernetics*, *32*, 114–121.

Chilali, M., & Gahinet, P. (1996). H_∞ Design with pole placement constraints: an LMI approach. *IEEE Transactions on Automatic Control*, *41*, 358–367.

Christensen, H. V. (2006). *Modelling and control of a twin-rotor MIMO system*. Technical Report Department of Control Engineering Institute of Electronic Systems of Aalborg University.

Coleman, T., Branch, M., & Grace, A. (2011). *Matlab Optimization Toolbox User's Guide (R2011b)*. The MathWorks, Inc.

Darus, I. Z. M., Aldebrez, F. M., & Tokhi, M. O. (2004). Parametric modelling of a twin rotor system using genetic algorithms. In *First International Symposium on Control, Communication and Signal Processing* (pp. 115–118).

Dutka, A. S., Ordys, A. W., & Grimble, M. J. (2003). Non-linear predictive control of 2 DOF helicopter model. In *42nd IEEE Conference on Decision and Control, Maui, Hawaii, USA*.

Franklin, G. F., Powell, J. D., & Workman, M. L. (1997). *Digital Control of Dynamic Systems*. (3rd ed.). Addison Wesley Longman.

Gabriel, C. (2008). *Modelling, simulation and control of a twin rotor MIMO system*. Master's thesis Department of Systems Engineering and Control of Universidad Politécnica de Valencia.

Ghersin, A. S., & Sanchez-Peña, R. S. (2002). LPV control of a 6 DOF vehicle. *IEEE Transactions on Control Systems Technology*, *10*, 883–887.

Groot Wassink, M., van de Wal, M., Scherer, C., & Okko Bosgra, O. (2005). LPV control for a wafer stage: beyond the theoretical solution. *Control Engineering Practice*, *13*, 231–245.

Gutman, S., & Jury, E. I. (1981). A general theory for matrix root clustering in subregions of the complex plane. *IEEE Transactions on Automatic Control*, *AC-26*, 853–863.

Kwiatkowski, A., Boll, M. T., & Werner, H. (2006). Automated generation and assessment of affine LPV Models. In *Proceedings of the 45th IEEE Conference on Decision and Control, San Diego, CA, USA* (pp. 6690–6695).

Lee, L. H., & Poolla, K. (1999). Identification of linear parameter varying systems using non linear programming. *Journal of Dynamic Systems, Measurements and Control*, *121*, 71–78.

Ljung, L. (1997). *Matlab System Identification Toolbox User's Guide (v. 4.0.3)*. The MathWorks, Inc.

Löfberg, J. (2004). YALMIP : a toolbox for modeling and optimization in MATLAB. In *Proceedings of the CACSD Conference*. Taipei, Taiwan.

López-Martinez, M., Díaz, J. M., Ortega, M. G., & Rubio, F. R. (2004). Control of a laboratory helicopter using switched 2-step feedback linearization. In *Proceedings of the 2004 American Control Conference, Boston, Massachusetts, USA*.

López-Martinez, M., Ortega, M. G., & Rubio, F. R. (2003). An H_∞ controller for a double rotor system. In *9th IEEE International Conference on Emerging Technologies and Factory Automation*.

López-Martinez, M., & Rubio, F. R. (2003). Control of a laboratory helicopter using feedback linearization. In *2003 European Control Conference, Cambridge, UK*.

López-Martinez, M., Vivas, C., & Ortega, M. G. (2005). A multivariable nonlinear H_∞ controller for a laboratory helicopter. In *44th IEEE conference on Decision and Control and European Control Conference, Seville Spain*.

Mäkilä, P. M., & Viljamaa, P. (2002). *Convex Parametric Design, Gain Scheduling, and Fuzzy Computing*. Technical Report Tampere, Tampere University of Technology, Institute of Automation and Control.

Mercere, G., Lovera, M., & Laroche, E. (2011). Identification of a flexible robot manipulator using a linear parameter-varying descriptor state-space structure. In *Proceedings of the Proceedings of the IEEE Conference on Decision and Control, Orlando, Florida, USA*.

Nejjari, F., Rotondo, D., Puig, V., & Innocenti, M. (2011). LPV modelling and control of a twin rotor MIMO system . In *19th IEEE Mediterranean Conference on Control and Automation*.

Nejjari, F., Rotondo, D., Puig, V., & Innocenti, M. (2012). Quasi-LPV modelling and non-linear identification of a twin rotor system . In *20th IEEE Mediterranean Conference on Control and Automation*.

Nemani, M., Ravikanth, R., & Bamieh, B. A. (1995). Identification of linear parametrically varying systems. In *Proceedings of the 34th IEEE Conference on Decision and Control, New Orleans, Louisiana, USA* (pp. 2990–2995). volume 3.

Packard, A. (1994). Gain scheduling via linear fractional transformation. *Systems and Control Letters*, *22*, 79–92.

Paijmans, B., Symens, W., Van Brussel, H., & Swevers, J. (2008). Identification of interpolating affine LPV models for mechatronic systems with one varying parameter. *European Journal of Control*, *14*, 16–29.

Papageorgiou, G. (1998). *Robust control system H_∞ loop shaping and aerospace application*. Ph.D. thesis Department of Engineering, University of Cambridge, Cambridge, England, U.K.

Rahideh, A., & Shaheed, M. H. (2007). Mathematical dynamic modelling of a twin-rotor multiple input-multiple output system. *Proceedings of the Institution of Mechanical Engineers, Part I: Journal of Systems and Control Engineering*, *221*, 89–101.

Rahideh, A., & Shaheed, M. H. (2009). Robust model predictive control of a twin rotor MIMO system. In *Proceedings of the 2009 IEEE International Conference on Mechatronics*.

Rahideh, A., Shaheed, M. H., & Huijberts, H. J. C. (2008). Dynamic modelling of a TRMS using analytical and empirical approaches. *Control Engineering Practice*, *16*, 241–259.

Reberga, L., Henrion, D., Bernussou, J., & Vary, F. (2005). LPV modeling of a turbofan engine. In *Proceedings of the 16th IFAC World Congress*.

Rodrigues, M., Theilliol, D., Aberkane, S., & Sauter, D. (2007). Fault tolerant control design for polytopic LPV systems. *International Journal of Applied Mathematics and Computer Science*, *17*, 27–37.

Rong, Q., & Irwin, G. W. (2003). LMI-Based Control Design for Discrete Polytopic LPV Systems. In *Proceedings of the 6th European Control Conference*.

Rugh, W. J., & Shamma, J. S. (2000). Research on gain scheduling. *Automatica*, *36*, 1401–1425.

Shaheed, M. H. (2004). Performance analysis of 4 types of conjugate gradient algorithm in the nonlinear dynamic modelling of a TRMS using feedforward neural networks. In *Proceedings of the 2004 IEEE International Conference on Systems, Man and Cybernetics* (pp. 5985–5990).

Shamma, J. S., & Cloutier, J. R. (1993). Gain-scheduled missile autopilot design using linear parameter varying transformations. *Journal of Guidance, Control, and Dynamics*, *16*, 256–263.

Steinbuch, M., van de Molengraft, R., & van der Voort, A. (2003). Experimental modelling and LPV control of a motion system. In *Proceedings of the 2003 American Control Conference, Denver, Colorado, USA* (pp. 1374–1379). volume 2.

Sturm, J. F. (1999). Using SeDuMi 1.02, a MATLAB toolbox for optimization over symmetric cones. *Optimization Methods and Software*, *11-12*, 625–653.

Sun, X. D., & Postlethwaite, I. (1998). Affine LPV modelling and its use in gain-scheduled helicopter control. In *UKACC International Conference on Control* (pp. 1504–1509).

Takagi, T., & Sugeno, M. (1985). Fuzzy Identification of Systems and Its Applications to Modeling and Control. *IEEE Transactions on Systems, Man, and Cybernetics*, *SMC-15*, 116–132.

Tao, C. W., Taur, J. S., Chang, Y. H., & Chang, C. W. (2010). A novel fuzzy-sliding and fuzzy-integral-sliding controller for the twin-rotor multi-input-multi-output system. *IEEE Transactions on Fuzzy Systems*, *18*, 893–905.

Toha, S. F., & Tokhi, M. O. (2009). Real-coded genetic algorithm for parametric modelling of a TRMS. In *Proceedings of the 11th conference on Evolutionary Computation (CEC)*.

Toha, S. F., & Tokhi, M. O. (2010a). ANFIS modelling of a twin rotor system using particle swarm optimisation and RLS. In *Proceedings of the 9th IEEE International Conference on Cybernetic Intelligent Systems*.

Toha, S. F., & Tokhi, M. O. (2010b). Parametric modelling application to a twin rotor system using recursive least squares, genetic, and swarm optimization techniques. *Proceedings of the Institution of Mechanical Engineers, Part G: Journal of Aerospace Engineering*, *224*, 961–977.

Toth, R., Abbas, H. S., & Werner, H. (2012). On the state-space realization of LPV input-output models: practical approaches. *IEEE Transactions on Control Systems Technology*, *20*, 139–153.

van Helvoort, J. J. M., Steinbuch, M., Lambrechts, P. F., & van de Molengraft, M. J. G. (2004). Analytical and experimental modelling for gain scheduling of a double scara robot. In *Proceedings of the 3rd IFAC Symposium on Mechatronic Systems, Sydney, Australia*.

van Wingerden, J. W., & Verhaegen, M. (2009). Subspace identification of bilinear and LPV systems for open- and closed-loop data. *Automatica*, *45*, 372–381.

Wan, Z., & Kothare, M. V. (2003). Efficient scheduled stabilizing output feedback model predictive control for constrained nonlinear systems. *IEEE Transactions on Automatic Control*, *49*, 331–346.

Wu, N. E., Zhang, Y., & Zhou, K. (2000). Detection, Estimation, and Accommodation of loss of Control Effectiveness. *International Journal Of Adaptive Control And Signal Processing*, *14*, 775–795.